Title	In Vitro Selection of Fluoroscent Signaling Peptide Aptamers Using Ribosome Display
Author(s)	Manandhar, Yasodha
Citation	
Issue Date	2015-03-25
URL	http://hdl.handle.net/10748/7145
DOI	
Rights	
Type	Thesis or Dissertation
Textversion	ETD

In Vitro Selection of Fluoroscent Signaling Peptide Aptamers Using Ribosome Display

YASODHA MANANDHAR

Department of Biological Sciences

Tokyo Metropolitan University

2015

Table of Contents

Abstract

Fluorescent signaling peptide aptamers are useful for biological science and diagnosis. In order to *in vitro* select the fluorescent signaling peptide aptamers, an environment sensitive fluorescent probe, 7-nitro-2,1,3-benzoxadiazole (NBD), was coupled with tRNA through aminophenylalanine and the tRNA was added during preparation of random sequence peptide library for ribosome display. By introduction of NBD as a side chain of non-natural amino acid into a library of random sequences, I successfully obtained fluorescent signaling peptide aptamers and investigated the interactions of selected peptides with the target molecule in detail.

I selected an aptamer against a target verotoxin which is a shiga-like toxin protein that causes mild diarrhea to life threatening hemolytic uremic syndrome. In addition, I investigated the interaction between the previously selected peptides with calmodulin (CaM).

The selected peptide aptamer against verotoxin showed change in fluorescence on interacting with verotoxin. This aptamer specifically interact with verotoxin and the dissociation constant (K_d) was 3.90 ± 1.6 μM. The fluorescence intensity of peptide aptamer was found to be decreased by 78% on increasing the verotoxin concentration. The selected peptides can be used for the detection of verotoxin.

On the other hand, the peptide aptamers against CaM showed enhancement in fluorescence by interacting with CaM in presence of calcium ions. The binding interactions of the selected peptide aptamers with CaM were investigated by nuclear magnetic resonance measurements, in addition to the surface plasmon resonance and fluorescence titration measurements.

List of Abbreviations

ssDNA	Single strand Deoxyribonucleic acid
DNA	Deoxyribonucleic acid
mRNA	Messenger ribonucleic acid
tRNA	Transfer ribonucleic acid
PCR	Polymerase chain reaction
RT-PCR	Reverse transcription polymerase chain reaction
SELEX	Systematic Evolution of Ligands by Exponential Enrichment
PRM	Peptide-ribosome-mRNA
EDTA	2,2',2",2"'-(Ethane-1,2-diyldinitrilo)tetraacetic acid
EGTA	Ethylene glycol tetraacetic acid
T7	T7 promoter
SD	Shine-Dalgarno
PS	Protein spacer
RBS	Ribosome binding site
PVF	Polyvinylidene fluoride membrane
UV	Ultraviolet
BSA	Bovine serum albumin
CaM	Calmodulin
NBD	7-Nitro-2,1,3-benzoxadiazole
NBDaa	NBD labeled phenylalanine
SPR	Surface Plasmon Resonance
NMR	Nuclear magnetic resonance
STD	Saturation-Transfer-Difference

CHAPTER 1

GENERAL INTRODUCTION

1-1 Background

"Aptamer" is the merge of two words 'aptus' meaning *fit* in Latin and 'meros' meaning *part* in Greek[1-3]. Aptamers are oligonucleotides (ribonucleic acid, RNA and single stranded deoxyribonucleic acid, ssDNA) or peptide molecules that can bind to their targets with high specifity and affinities (picomolar to nano molar dissociation constants)[4]. They are also known as artificial or chemical antibodies which has attracted the attention of many scientists due to their unique merits over antibodies such as thermal stability, low cost and unlimited applications[5-9].

Peptide aptamers previously known as combinatorial proteins inserted into a constant scaffold protein[10-12]. They were for the first time selected using phage display technique[13,14]. This technique is a molecular approach to express proteins or peptides on the surface of phage particles with the genetic information of these proteins or peptides encoding inside[15]. It expresses natural and random peptides, proteins as well antibody fragments. This technique was used to convert nucleotide sequences into peptides and proteins of desired properties[16].

Initially peptide aptamers were developed as research tools to dissect protein function within complex molecular regulatory networks[17]. These typically contain 8-20 amino acids. They can be engineered via selection from large libraries of random sequences by direct evolution techniques. Not only are the aptamers important for guide and self-assembly of large materials but they are valuable in single molecule assay design[18]. They bind to their target proteins with significant affinity and high specificity, both *in vitro* and *in vivo*[3]. They comprises the important assemblage in the field of aptamers as short peptide has the ability to mimic the interactive features of large and complex counterparts[19].

They offer means of high-confidence, ligand-based target validation and can exhibit different specificity profiles towards a protein family. This particular property might prove to be important because the concept of 'multi-targeting' promises to be a fruitful avenue for drug discovery and development especially when addressing protein families whose members exhibit functional redundancy[20]. To develop peptide-derived drugs that can be applied in a general medical setting, several issues (potential immunogenicity, protease degradation and poor metabolic stability) remain to be resolved for human administration. The emergent peptide binders that overcome the above difficulties will allow us to tailor peptide drugs for the prevention, diagnosis and treatment of a wide variety of diseases[21].

Now various approaches are established to generate functional aptamers. Some classical examples are phage display[22-24], bacterial surface display[25], yeast display[26-29], mRNA display[29-33] and ribosomal display[34-35]. Adaptation of the approach depends on the type of aptamer and its application. All these approaches have their merits and limitations. In case of phage display, bacterial surface display and yeast display require transformation of living cells limits number of independent libraries. In addition, due to requirement of living cell restrict the condition applicable for infectious virus. The Systematic Evolution of Ligands by Exponential Enrichment (SELEX) process is limited to generate oligonucleotide aptamer. The main feature of all *in vitro* selection approaches is combination of genotype messenger RNA (mRNA) and phenotype (peptide). This genotype and phenotype conjugation play role to know the genetic information of the binding aptamer generated from the random library. Thus the formation of stable complex between genotype and phenotype is essential for the proper selection of aptamer. This stable complex can be achieved in the ribosomal

display technique. Moreover ribosomal display technique has other advantages over other approaches. First, the diversity of the library is not limited by the transformation efficiency of bacterial cells, but only by the number of ribosomes and different mRNA molecules present in the test tube. Second, random mutations can be introduced easily after each selection round. Thus, I used ribosomal display technique to select the desired peptide aptamers.

1-2 Ribosome Display

Ribosome display is a cell-free system for the *in vitro* selection of proteins and peptides from large libraries[36-37]. It provides a prevailing technology to ascertain specific, high affinity aptamers from large random libraries. In this technique no transformation step is required and suitable for generating toxic, proteolytically sensitive and unstable proteins as well can incorporate non-natural amino acids at defined positions[38].

The first published description of ribosome display was for peptide selection using a coupled *E. coli* S30 system and termed 'polysome display'. To perform this approach a library containing DNA constructs devoid of STOP-codons (UAA, UAG or UGA) is *in vitro* transcribed to yield library mRNA. After the transcription generally translation takes place in a four-step cycle (Figure 1).

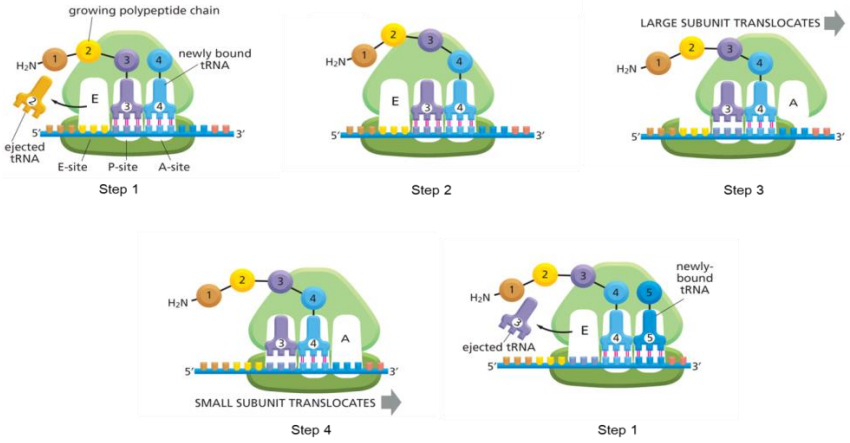

Figure 1: Translation cycle[39].

This cycle repeat over and over during the synthesis of a protein. In step 1, a transfer RNA (tRNA) carrying the next amino acid in the chain binds to the vacant A-site on the ribosome by forming base pairs with the codon that is exposed there. As only one of the many types of tRNA molecules in a cell can base-pair with each codon, this new codon determines the specific amino acid to be added to the growing polypeptide chain. The A and P sites are sufficiently close and this positioning of the tRNA ensures that the correct reading frame will be preserved throughout the synthesis of the protein. In step 2, the carboxyl end of the polypeptide chain is uncoupled from the tRNA at the P site and joined by a peptide bond to the free amino group of the amino acid linked to the tRNA at the A site. The enzymatic site in the large subunit catalyzes this reaction. In step 3, a shift of large subunit moves the two tRNAs into the E and P sites of large subunit. In step 4, the small subunit moves three nucleotides along the mRNA molecule, bringing it back to its original position relative to the large subunit. This movement creates an empty A site for the next aminoacyl-tRNA molecule to bind. mRNA is translated in the 5'- to -3' direction and N-terminal end of a protein is made first with each cycle adding one amino acid to the C-terminus of the polypeptide chain.

In normal condition the release of the polypeptides from the ribosome is signaled by the presence of stop codons. Release factor, a protein, bind to any stop codon present on A site of ribosome and this binding catalyze the addition of water molecule instead of amino acid by altering the activity of peptidyl transferase (Figure 2 A). Due to the absence of a STOP-codon in library, ribosomal translation goes to the end of the mRNA molecules (Figure 2 B). The mRNA molecule, ribosome and newly synthesized polypeptide stay physically attached in a ternary complex. The addition of Mg^{2+} ions increase the stability of the translated nascent proteins with the corresponding mRNA, through the formation of stable protein–ribosome–mRNA (PRM) complexes[39].

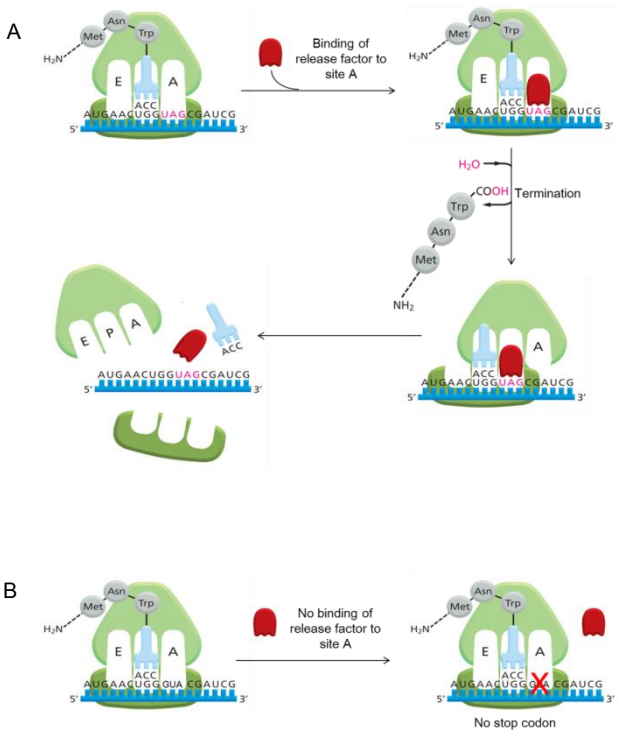

Figure 2: A. The binding of a release factor to site A bearing stop codon terminates translation, the final phase of protein synthesis. B. In the absence of stop codon, the release factor can't bind to site A forming the peptide, ribosome and mRNA complex[39].

These complexes enter a selection cycle to expose on the immobilized target. After each selection cycle, mRNA molecules of captured ternary complexes are reverse transcribed and amplified in a PCR reaction to generate template for the next selection cycle as shown in figure 3[34-35]. This permits the simultaneous isolation of a functional nascent protein, through affinity for a ligand, together with the encoding mRNA, which is then converted and amplified as DNA for further manipulation including repeated cycles or protein expression from a 10^{12} member DNA library[40].

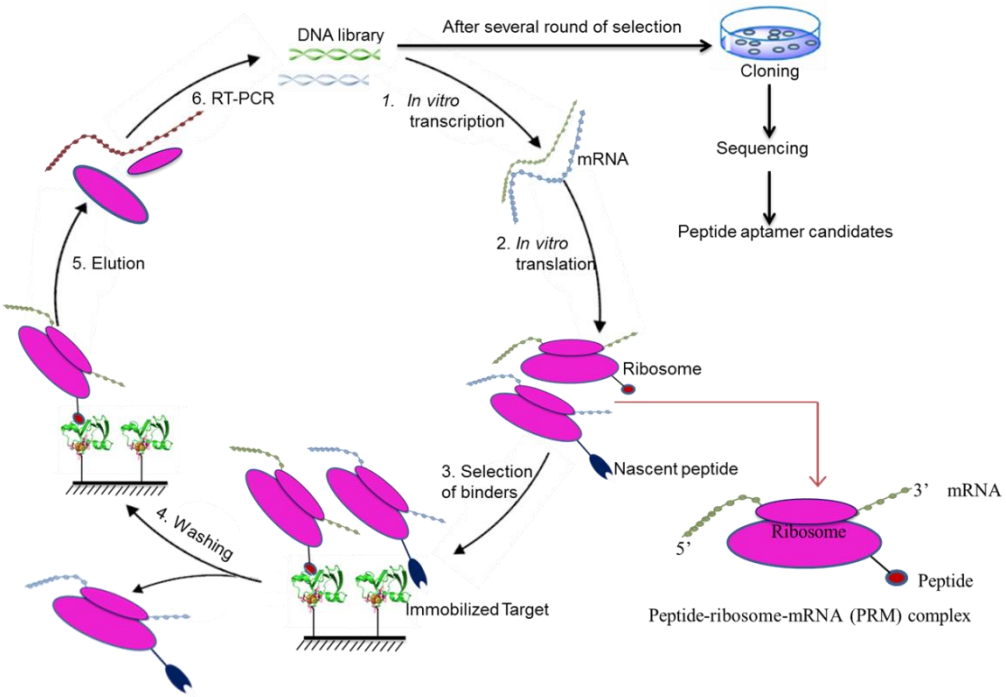

Figure 3: Illustration of a typical ribosome display selection cycle. A library of linear DNA fragments devoid of STOP-codons is *in vitro* transcribed to yield library mRNA which on its part is *in vitro* translated. The absence of a STOP-codon and addition of Mg^{2+}-ions stalls ribosomes on their cognate mRNA and yields ternary complexes of mRNA, ribosome and displayed protein. These complexes are then exposed to an immobilized target, non-binding complexes are washed away and the mRNA of binding complexes is eluted and isolated upon addition of the Mg^{2+}, chelator EDTA. Isolated mRNA is reverse transcribed and PCR-amplified for next selection cycle or post-selection analysis.

Several issues need to be addressed to select the functional peptides against the target molecules using ribosome display technique. Library construct typically consists of a T7 promoter that allows for mRNA synthesis, followed by a ribosome binding site (RBS) that can base-pair with ribosomal RNA, thus recruiting the ribosome to the downstream start codon (AUG) where protein synthesis is initiated. The open reading frame frequently starts with a protein detection tag such as the RGS-His6 tag or the FLAG tag, followed by the library of binding proteins and a spacer protein. A spacer domain of at least 23–30 amino acids' length is required at the C terminus, to allow the protein to exit completely from the ribosome 'tunnel' and the translated protein must be fold correctly into its three-dimensional structure to bind with the target molecule[41-43]. Another important issue is stability of the PRM complex together during selection. The complex is important for the enrichment of the selection, which contains the genetic information of the peptide aptamers as well keep ribosomal subunit together. Where large subunit catalyzes peptide bond formation to enable the complete nascent protein and small subunit mediates the interactions between mRNA and tRNAs that determine the sequences of the proteins translated.

Figure 4: Schematic diagram of the DNA library for ribosome display technology. Here, T7 denotes the T7 promoter for *in vitro* transcription; SD, the Shine Dalgarno sequence for *in vitro* translation followed by random sequence containing 8-20 random residues; SP, spacer protein which is a part of protein construct which connects the folded random sequence to ribosome.

The selection results in gradual enrichment of the library with sequences exhibiting the increased affinity to the target. Usually after successful selection, the affinity of the library to the target increases by several orders of magnitude. On average, from 5 to 15 rounds of selection is sufficient to obtain aptamers. However in some cases a significant enrichment of the library with sequences specific of the target protein becomes noticeable already after the first rounds of selection[44-46]. After cessation of affinity increase, the enriched library is cloned and sequences of individual aptamers are determined[47].

1-2-1 Use of ribosome display

Ribosome display has been used to produce proteins/peptides consisting of not only natural but also unnatural amino acids in combination with chemically modified amino acyl-tRNAs[48-49]. Thus, using this technique can incorporate the fluorogenic compound in the peptide aptamers which are useful for diagnosis purposes. Various types of peptide binders have been selected with such technologies for use in a wide range of fields from bioscience to medicine[50-58].

The ingenuousness of ribosome display allows for the introduction of additional diversity in between selection cycles using error-prone PCR or by gene shuffling. This feature makes ribosome display a dynamic selection system that can mimic the natural affinity maturation process of antibodies where somatic mutations introduce additional diversity during the development of B-cells. It is reported that the selection and evolution of scFv antibody fragments with equilibrium dissociation constants as low as 82 pM when combining ribosome display with error-prone PCR. The introduced point mutations accounted up to 40-fold increase in affinity as compared

to the progenitor clones[59]. In another study, the combination of error-prone PCR and gene shuffling in subsequent cycles yielded an increased population of affinity-improved variants, and the highest affinity clone, as compared to error-prone PCR only[60].The introduced point mutations accounted for an up to 40-fold increase in affinity as compared to the progenitor clones[59]. In another study, the combination of error-prone PCR and gene shuffling in subsequent cycles yielded an increased population of affinity-improved variants, and the highest affinity clone, as compared to error-prone PCR only[60].

1-3 Applications

Aptamers based drugs are presently under clinical tests, and the first drug (Macugen) has already appeared on the pharmaceutical market[61]. *In vivo* experiments demonstrate that they generally exhibit low toxicity and immunogenicity characteristics, which make them suitable for therapeutic use[50, 62-63] . They can be used in search for new inhibitors of different proteins, for this, one can perform a directed search for molecules, competing with the aptamer inhibitor for binding to the protein target and thus interacting with the same site of the protein as the original aptamer[7]. They are widely used for detection of different target molecules (in particular, for diagnostic purposes). It was shown that aptamers could successfully replace antibodies in methods of ELISA, fluorescent hybridization in situ, western blotting, etc[64-65]. Aptamers also used for measuring concentrations of various metabolites and protein factors, for detection of toxins, revealing specific types of cells and tissues, and cells of pathogenic microorganisms[18, 66-69]. Thus, aptamers can be applied as research tools, biosensors,

therapeutic agents and so on. Relying on these properties, I designed biomarkers for proteins by incorporating artificial amino acid coupled t-RNA using ribosome display.

The incorporation of the non-natural amino acids into the selected peptide aptamers adds new artificial functions to the aptamers which ultimately improve the applications. The kinds of unnatural component important to improve the functions of the aptamers are photo-isomerizable, fluorogenic or inhibitor. Incorporation of these compounds into the peptide aptamers depend on its application. Specifically, addition of the fluorescence signaling compound is the most promising approach, because the fluorescence signal measurement technique is most sensitive and reliable to check the interaction between target and aptamers. I selected the signaling peptide aptamers consisting environmental sensitive dye 7-Nitro-2, 1, 3-benzoxadiazole (NBD) which changes fluorescence depending on the surrounding environments. Binding of dye in hydrophobic pocket enhances the fluorescent intensity but on hydrophilic domain decreases the fluorescent intensity. The environmental sensitive dye NBD was incorporated by the combination of ribosomal display and bio orthogonally prepared tRNA.

In the coming chapters, I will be dealing in detail about the selections of peptide aptamer containing fluorogeninc dye NBD against the targets verotoxin and calmodulin. The binding of the selected aptamers against them and their potential application will also be covered.

References

1. Ellington AD, Szostak JW. *In vitro* selection of RNA molecules that bind specific ligands. *Nature* 346, 1990, pp 818-822.
2. Tuerk C and Gold L. Systematic evolution of ligands by exponential enrichment: RNA ligands to bacteriophage T4 DNA polymerase. *Science* 249, 1990, pp 505-510.
3. Seyler FH, et al. Peptide aptamers: specific inhibitors of protein function. *Current molecular medicine*. 4, 2004, pp 529-538.
4. Lee JF, et al. Aptamer therapeutics advance. *Science,* 10, 2006, pp 282-289.
5. Carlson B. Aptamers: the new frontier in drug development? *Biotechnology healthcare*, 2007, pp 31-36.
6. Song S, et al. Aptamer-based biosensors. *Trends in analytical chemistry*, 27, 2008, pp 108-117.
7. Johnson S, et al. Surface-Immobilized peptide aptamers as probe molecules for protein detection. *Anal. Chem.* 80, 2008, pp 978-983.
8. Song KM, et al. Aptamers and their biological applications. *Sensors*, 12, 2012, pp 612-631.
9. Stalin C. and Dineshkumar P. Aptamers role in basic drug research and development-an overview. *Int. J. Pharmacy and Pharmaceutical sciences*, 4, 2012, pp35-42.
10. Mascini M, et al.Nucleic acid and peptide aptamers: fundamentals and bioanalytical aspects. *Angew Chem Int*. 51, 2012, pp 1316-1332.
11. Conidi A, et al. Aptamers and Their Potential to Selectively Target Aspects of EGF, Wnt/beta-Catenin and TGFbeta-Smad Family Signaling. *Int J Mol Sci*. 14, 2013, pp 6690-6719.
12. Colas P, et al. Genetic selection of peptide aptamers that recognize and inhibit cyclindependent kinase 2. *Nature*, 380, 1996, pp 548-550.
13. Smith GP. Filamentous phage fusion: novel expression vectors that display cloned antigens on the surface of the viron. *Science*, 228, 1985, pp 1315–1317.

14. Smith GP and Petrenko VA. Phage display. *Chem Rev.*, 97, 1997, pp 391-410.

15. Pande J, et al. Phage display: concept, innovations, applications and future. *Biotechnol Adv*, 28, 2010, pp 849-858.

16. Willats WGT. Phage display: practicalities and prospects. *Plant molecular biology*, 50, 2002, pp 837-854.

17. Colas P, et al. Genetic selection of peptide aptamers that recognize and inhibit cyclin-dependent kinase 2, *Nature*, 380, 1996, pp 548-550.

18. Tam AEA, et al. Adhesion through single peptide aptamers. *J. Phys. Chem. A.*, 2010.

19. Tonelli RR, et al. Selection of binding targets in parasites using phage-display and aptamer libraries *in vivo* and *in vitro*. *Frontiers in immunology*. 3, 2013, pp 1-16.

20. Baines IC and Colas P. Peptide aptamers as guides for small-molecule drug discovery. *DDT*. 11, 2006, pp 334-341.

21. Wada A. Development of next-generation peptide binders using *in vitro* display technologies and their potential applications. *Frontiers in immunology*, 4, 2013, pp 1-6.

22. Scott KK and Smith GP. Searching for peptide ligands with an epitope library. *Science*, 249, 1990, pp 386-390.

23. Bass S, et al. Hormone phage: an enrichment method for variant proteins with altered binding properties. *Proteins*, 8, 1990, pp 309-314.

24. Clackson T, et al. Making antibody fragments using phage display libraries. *Nature*, 352, 1991, pp 624-628.

25. Wernerus H, et al. Generation of metal-binding Staphylococci through surface display of combinatorially engineered cellulose-binding domains. *Appl. Environ. Microbiol.*, 67, pp 4678-4684.

26. Boder ET and Wittrup KD. Yeast surface display for screening combinatorial polypeptide libraries. *Nat. Biotechnol*., 15, 1997, pp 553-557.

27. Seyler FH, et al. Peptide aptamers: specific inhibitors of protein function. *Current molecular medicine*, 4, 2004, pp 529-538.

28. Crawford M, et al. Peptide aptamer: tools for biology and drug discovery. *Briefing in functional genomics and proteomics*, 2, 2003, pp 72-79.

29. Bowley DR, et al. Antigen selection from an HIV-1 immune antibody library displayed on yeast yields many novel antibodies compared to selection from the same library displayed on phage. *Protein Eng. Des. Sel*., 20, 2007, pp 81-90.

30. Roberts RW and Szostak JW. RNA-peptide fusions for the *in vitro* selection of peptides and proteins. *Proc. Natl Acad. Sci. USA*, 94, 1997, pp 12297-12302.

31. Keefe AD and Szostak JW. Functional proteins from a random-sequence library. *Nature*, 410, 2001, pp 715-718.

32. Seelig B and Szostak JW. Selection and evolution of enzymes from a partially randomized non-catalytic scaffold. *Nature*, 448, 2007, pp 828-831.

33. Shen X, et al. Scanning the human proteome for calmodulin-binding proteins. *Proc. Natl. Acad. Sci. USA*, 102, 2005, pp 5969-5974.

34. Mattheakis LC, et al. An *in vitro* polysome display system for identifying ligands from very large peptide libraries. *Proc. Natl. Acad. Sci. USA*, 91, 1994, pp 9022-9026.

35. Hanes J and Pluckthun A. *In vitro* selection and evolution of functional proteins by using ribosome display. *Proc. Natl. Acad. Sci. USA*, 94, 1997, pp 4937-4942.

36. Zahnd C, et al. Ribosome display: selecting and evolving proteins in vitro that specifically bind to a target. *Nat. Methods*, 4, 2007, pp 269–279.

37. Mattheakis LC, et al. An *in vitro* polysome display system for identifying ligands from very large peptide libraries. *PNAS*, 91, 1994, pp 9022–9026.

38. He M and Taussig MJ. Ribosome display: cell-free protein display technology. *Brief Funct Genomic*

Proteomic., 2, 2002, pp 204-212.

39. Hopkin AB, et al. From DNA to protein: How cells read the genome. *Essential cell biology*, third edition, chapter 7, Garland science, Taylor and Francis group, New York and UK, 2010, pp 231-267.
40. Mattheakis LC, et al. An *in vitro* polysome display system for identifying ligands from very large peptide libraries. *PNAS*, 91, 1994, pp 9022–9026.
41. He M and Taussig MJ. Ribosome display: cell free protein display technology. *Briefings in functional genomics and proteomics*, 1, 2002, pp 204-212.
42. Moore PB and Steitz TA. The involvement of RNA in ribosome function. *Nature*, 418, 2002, pp 229-235.
43. Makeyev EV, et al. Enzymatic activity of the ribosome-bound nacent polypeptide. *FEBS Lett.*, 378, 1996, pp 166-170.
44. Fitter S and James R. Deconvolution of a Complex Target Using DNA Aptamers. *J. Biol. Chem.*, 280, 2005, pp 34193-34201.
45. Berezovski M, et al. Nonequilibrium Capillary Electrophoresis of Equilibrium Mixtures: A Universal Tool for Development of Aptamers. *JACS*, 127, 2005, pp 3165-3171.
46. Bianchini M, et al. Specific oligobodies against ERK-2 that recognize both the native and the denatured state of the protein. *J. Immunol. Meth.*, 252, 2001, pp 191-197.
47. Nutiu R and Li Y. Aptamers with fluorescence-signaling properties. *Methods*, 37, 2005, pp 16-25.
48. Josephson K, et al. Ribosomal synthesis of unnatural peptides. *JACS*, 127, 2005, pp 11727–11735.
49. Kajihara D, et al. FRET analysis of protein conformational change through position specific incorporation of fluorescent amino acids. Nat. Methods, 3, 2006, pp 923–929.
50. Kulbachinskiy AV. Methods for selection of aptamers to protein targets. *Biochemistry*, 72, 2006, pp1505-1518.
51. Cwirla SE, et al. Peptide agonist of the thrombopoietin receptor as potent as the natural cytokine.

Science 276, 1997, pp 5319-1696.

52. Su JL, et al. A novel peptide specifically binding to interleukin-6 receptor (gp80) inhibits angiogenesis and tumor growth. *Cancer Res*. 65, 2005, pp 4827–4835.
53. Hyde DRR, et al. Detection of small-molecule enzyme inhibitors with peptides isolated from phage-displayed combinatorial peptide libraries. *Chem. Biol.*, 7, 2000, pp 17–25.
54. Welch BD, et al. Potent D-peptide inhibitors of HIV-1 entry. *PNAS*, 104, 2007, pp 16828–16833.
55. Matsubara T, et al. Sialic acid-mimic peptides as hemagglutinin inhibitors for anti-influenza therapy. J. Med. Chem., 53, 2010, pp 4441-4449.
56. Whaley SR. Selection of peptides with semiconductor binding specificity for directed nanocrystal assembly. *Nature*, 405, 2000, pp 665–668.
57. Wang S, et al. Peptides with selective affinity for carbon nanotubes. *Nat. Mater*, 2, 2003, pp 196–200.
58. Rodi DJ, et al. Screening of a library of phage-displayed peptides identifies human bcl-2 as a taxol-binding protein. *J. Mol. Biol*., 285, 1999, pp 197–203.
59. Hanes J, et al. Picomolar affinity antibodies from a fully synthetic naïve library selected and evolved by ribosome display. *Nat. Biotechnol.*, 18, 2000, pp 1287-1292.
60. Matthieu C, et al. *In vitro* DNA recombination by L-Shuffling during ribosome display affinity maturation of an anti-Fas antibody increases the population of improved variants. *Protein Eng. Des. Sel.*, 21, 2008, pp 343-351.
61. Drabovich AP, et al. Smart aptamers facilitate multi-probe affinity analysis of proteins with ultra-wide dynamic range of measured concentrations. *JACS*, 129, 2007, pp 7260-7261.
62. Morse DP. Direct selection of RNA beacon aptamers. *Science,* 359, 2007, pp 94-101.
63. Li N and Ho CM. Aptamer –based optical probes with separated molecular recognition and signal transduction modules. *JACS*, 30, 2008, pp 2380-2381.

64. Gerald KF. *In vitro* display technologies-new tools for drug discovery. *DDT*, 5, 2000, pp 253-258.

65. Stojanovic MN and Landry DW. Aptamer-based colorimetric probe for cocaine. *JACS*, 124, 2002, pp 9678-9679.

66. Oh SS, et al. *In vitro* selection of structure-switching, self-reporting aptamers. *PNAS*, 107, 2010, pp 14053-14058.

67. Jhaveri S, et al. *In vitro* selection of signaling aptamers. *Nature Biotechnology*, 18, 2000, pp 1293-1297.

68. Paige JS, et al. RNA mimics of green fluorescent protein. *Science*. 333, 2011, pp 642-646.

69. Chen X. Protein and peptide probes for molecular imaging. *Amino acids*, 41, 2011, pp 1009-101

CHAPTER 2

IN VITRO SELECTION OF A PEPTIDE APTAMER THAT CHANGES FLUORESCENCE IN RESPONSE TO VEROTOXIN

2-1 Introduction

Antibodies are now widely used for various applications, including medical diagnostics and environmental analysis[1]. However, the main function of antibodies is to bind to their target molecules. Unfortunately, cumbersome processes are required to quantify the amount of target-bound antibodies for diagnostic applications. To develop a separation-free sensor that provides a quantitative signal upon binding to its target, here in I describe *in vitro* selection or so-called "molecular evolutionary engineering", which offers great potential to engineer an artificial antibody (aptamer)[2-5].

Oligonucleotide-based signaling aptamers have been reported since the development of *in vitro* selection. However, a peptide-based signaling aptamer that has greater functional diversity when compared with oligonucleotides may facilitate the development of an aptamer with higher affinity and specificity. In the case of a peptide aptamer, the selection has been performed from biologically expressed libraries, such as phage, although, molecular level expression via a bioorthogonal evolution method, such as ribosome or mRNA display, has also been achieved[6-11]. Recently, it was reported that an artificial amino acid carried by a tRNA molecule could be incorporated into a translated peptide via a cell-free protein synthesis system[12-14].

To confirm the universality of chemically extended *in vitro* selection, I have to demonstrate aptamers to arbitrary targets using developed bioorthogonal evolution method. In this research, I selected verotoxin as the target (Figure 1A).

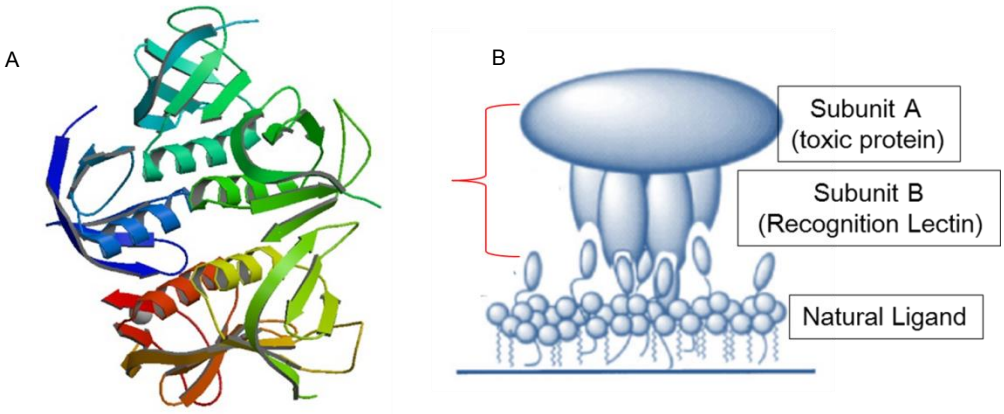

Verotoxin[15] **Verotoxin with natural ligand**[16]

Figure 1: Verotoxin

Verotoxin, a virulence factor of *Escherichia coli* strains that produce cytotoxin for vero cells was discovered in 1977. They also known as Shiga-like toxin, belong to AB_5 family of toxins comprising of A (an enzymatically active and toxic) subunit and five identical B (receptor binding portion of the molecule) subunits which allows pentameric attachment to the cell surface receptors (Figure 1B). The A subunit in this toxin is responsible for inhibiting protein synthesis through the catalytic inactivation of 60S ribosomal subunits, leading to inhibition of aminoacyl – tRNA binding in the peptide elongation reaction and these toxins are endocytosed via clathrin-coated or uncoated pits to the cytosol by the B subunit[17-23]. The mature subunit A of this protein comprises of 293 amino acids whereas each monomer of B subunit consist of 69 amino acids. The total amino acid present in this protein is 638 with the molecular weight of 70677 Da (A: 32217 Da + B: 7692 X 5)[24].

In this protein, subunit A is situated on the face of the subunit B lectins (homopentameric protein) and its C-terminus is anchored in a central pore of subunit B[25] (Figure 2A). The B subunit comprises two three stranded antiparallel β–sheets and an

α–helix. The functional receptors of verotoxin 1 on the cell surface are glycolipid, globotriosylceramide (Gb_3; Gal (α1-4) Gal (β1-4) GlcCer) and globotetraosylceramide, Gb_4. The crystal structure of the verotoxin B pentamer complexed with a Gb_3 analogue revealed the existence of three Gb_3-binding sites per B-subunit (i.e. 15 binding sites per B-pentamer) as shown in Figure 2B. The carbohydrate-binding sites are occupied by residues with polar and acidic side chains which helps in hydrogen bonding with polar groups[17, 27-32].

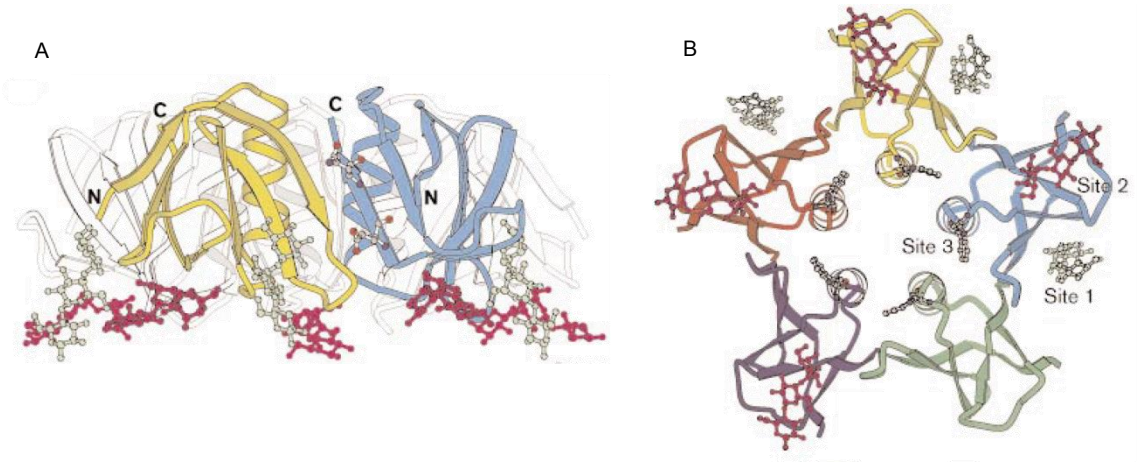

Figure 2: A. The side view of B subunit facing the receptor-binding surface at the bottom. B. Three Gb_3-binding sites per B subunit with each monomer shown in different colour[26] .

Hydrophobic interactions occur at site 1 whereas at site 2, the presence of three sugar residues facilitate interaction by hydrogen bonding and site 3, the trisaccharide chain encourages hydrophobic interactions[31]. The binding constant for the soluble trisaccharide of Gb_3 to the soluble form of the pentameric subunit B was found to be relatively weak (milli molar) per one monomer[33-34].

The verotoxicity increases in the presence of Ca^{2+} and EDTA where as Fe^{3+} reduced the production of verotoxin 1. The toxicity was found to be stable for up to 60 min at 70 °C (i.e. heat–stable toxin) but at pH 4.5, 90 % activity was found to be reduced.

The isoelectric point of verotoxin 1 was found to be 7.03. On checking the pI of separate subunits pI of A was found to be 11.1 and of B was found to be 5.9. Less than 1 pg of toxin per mL of culture medium was found to be enough to kill sensitive cells overnight[18, 35-36]. Most of the occurrences of infections leading to wild outbreaks in the world is due to the food and water borne transmission[37-38].

The major symptoms seen when infected by this toxin were abdominal pain, diarrhea, fever and later developed bloody diarrhea followed by epidemics of hemorrhagic colitis and the hemolytic-uremic syndrome (HUS)[39]. The HUS directly induces kidney damage and is the major cause of renal failure in children. Some clinical results suggest that conventional antimicrobial therapies are not useful and even may be counterproductive so there is a great need to develop new therapies to treat the diseases[20].

For the detection of the toxin several methods such as PCR (of clinical samples, feces, fecal broth cultures)[40], SPR (Immobilizing the peptide nucleic acid on the sensor chip and toxin genes as analyte)[41-42], immunochromatographic test (Duopath verotoxins GLISA), antibody capture[37], bioluminescent enzyme immunoassay[43] have been developed. However, these methods are time consuming.

For the treatment of the infection caused by this toxin, many researches are going on such as binding site inhibition[44-45], neutralization of toxins[46]. Currently a multi targeted approach like multi drug therapy is practiced[47-48] and a drug Synsorb-Pk has completed the phase III randomized study[49-50].

For the treatment of the infection, prompt and adequate detection techniques are required so that the retrospective and prospective control of infection can be done. Thus,

in this research, I sought to engineer peptide aptamers by employing ribosome display (Figure 4) and a tRNA carrying a fluorescent probe, 7-nitro-2,1,3-benzoxadiazole (NBD), of which fluorescence considerably depends on the environment.

2-2 Materials and Methods

2-2-1 Materials

Verotoxin (Denka Seiken Co. Ltd., Japan)[51]

Single strand DNA library (ssDNA), primers was synthesized by Operon, Japan.

The library has T7 promoter then ribosomal binding site followed by random sequence, which is the mixture of $(VVN)_{10}$, $(NNH)_{10}$ and $(NNY)_{10}$, where V is A, G or C; N is A, T, G or C; H is A, T or C and Y is C or T with tol A linker followed by Sec M.

Fwd Primer-1: Fwd T7 TolA long 120719, 5'-TAATACGACTCACTATAGGGCAGAAGCAAGGGCGGCACTTTAAG-3'

Fwd Primer-2: Fwd M13_120117), 5'-GTAAAACGACGGCCAG-3'

Rev Primer-1: Rev TolA 110617), 5'-TTAGCTCACCGAAAATATCATCTG-3'

Rev Primer-2: (Geneart RevB 120106), 5'-GCGAAAGCGGCGGCAGATG-3'

Rev Primer-3: (Rev M13_120117), 5'-CAGGAAACAGCTATGAC-3'

Nunc-plate (Thermo Fisher Scientific, Denmark)

GelCode® blue stain reagent (Thermo scientific, USA)

T7 RiboMAX™ Express Large Scale RNA Production System (Promega, USA)

TURBO DNase (Ambion, USA)

RNA Clean and Concentrator TM-25 (Zymo Research, USA)

E-gel® GO (Invitrogen, Israel)

Prime STAR® GXL DNA polymerase (Takara, Japan)

RNase inhibitor RNasin (Promega, USA)

DNA Ligation kit (Takara, Japan)

PrimeScript™ Reverse Transcriptase (Takara, Japan)

Pure System®, Classic II 96 kit (BioComber Co. Ltd., Japan)

Zero Blunt® TOPO® PCR cloning kit (Invitrogen, USA)

Nucleo Spin Gel and PCR Clean up (Macherey-Nagel, Germany)

NucAway ™ Spin Columns (Ambion Inc., USA)

KOD plus Neo (Toyobo, Japan)

Agarose LO3 (Takara, Japan)

Bovine serum albumin (Equitech-Bio Inc., USA)

Gelatin, bovine (Sigma, USA)

IgG, rabbit (Sigma, USA)

β-Lactoglobulin, bovine (Sigma, USA)

Ovalbumin (Sigma, USA)

Rink Amide MBHA resin (Novabiochem, China)

N-methyl-2-pyrrolidone, NMP (Wako Pure Chem. Ind. Ltd., Japan)

Piperidine (Wako Pure Chem. Ind. Ltd., Japan)

N-ethyldiisopropylamine (Wako Pure Chem. Ind. Ltd., Japan)

1-[bis(dimethylamino)methylene]-1H-1,2,3-triazolo[4,5-b]pyridinium 3-oxid hexafluorophosphate (AnaSpec Inc., USA)

ECL Advance™ blocking agent (GE, UK)

Polyvinylidene fluoride membrane (Merck, USA)

Selection buffer: 50 mM Tris-acetate, 150 mM NaCl, 50 mM magnesium acetate and 0.05 % Tween® 20, pH 7

Elution buffer: 50 mM Tris-acetate, 150 mM NaCl, 50 mM EDTA, pH 7

TBST buffer: 50 mM Tris-HCl, 150 mM NaCl, 0.05 % Tween® 20, pH 7

Blotting buffer: 25 mM Tris-HCl, 192 mM Glycine, 20 % Methanol

Blocking buffer: 4 % Blocking agent in TBST

NBD-C6-AF-tRNA, CoverDirect tRNA reagents for site-directed protein labeling, Protein Express, Chiba, Japan

2-2-2 Methods

2-2-2-1 Immobilization of verotoxin for affinity selection

The target protein verotoxin was immobilized on Nunc-plates. These plates were washed with TBS buffer (300 µL X 3) then different concentrations (1, 5 and 10 µM) of verotoxin were added in the plates. Plates were covered with paraffin films and left on shaker at 4 °C (25 rpm) overnight. The wells were washed with milliQ water and stained by GelCode® blue stain reagent for 2 hours. After staining, the wells were washed with milliQ water and the presence of blue stain was checked. By comparing the stain result, 5 µM concentration immobilized plates were used for the selection.

2-2-2-2 In vitro selection

a. Construction of DNA template

The DNA template for *in vitro* selection was designed (Figure 3). The sequence encompasses of T7 promoter (5'-TAATACGACTCACTATA-3') for *in vitro* transcription; SD, a Shine Dalgarno *E. Coli* ribosome binding site sequence; random sequence; TolA linker as a protein spacer followed by Sec M for the pause of ribosome.

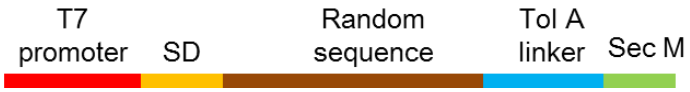

Figure 3: Structure of DNA template

The random sequence consist of VVN, NNY and NNH sequence with amber codon (TAG, for the incorporation of non-natural amino acid), where V: A, G or C; N: A, T, G or C; H: A, T or C and Y: C or T. During selection these 3 different library sequences were mixed in equimolar concentration.

b. In vitro transcription and translation

The DNA template was transcribed and translated. The transcription was performed at 37 °C overnight using RiboMAX large scale RNA production system. Next day, reaction was stopped by adding DNase for complete inhibition of template DNA and incubating the mixture for 30 min. The mRNA was purified by using Zymo RNA purification kit and translation was conducted using Pure System® Classic II 96 in the presence of NBD coupled phenylalanine-carrying tRNA, which was synthesized as described previously[52]. The mixture was incubated at 37 °C for 15 min then mixture was placed on ice for 10 min to stop the translation reaction.

c. Affinity selection and recovery of mRNA

200 µL of the selection buffer (50 mM Tris-acetate, 150 mM NaCl, 50 mM magnesium acetate and 0.05 % Tween 20, pH 7) was added to the reaction mixture of 50 µL (i.e. dilution for 5 times was done to the translated solution). Then this solution was added to Nunc-plate and incubated at 4 °C for 1 h. After the plate washed five times with ice cold selection buffer, elution was carried out by adding 50 µL of the elution buffer (50 mM Tris-acetate, 150 mM NaCl, 50 mM EDTA, pH 7) till 3rd round of selection. From 4th to 8th round, elution was performed using verotoxin. The concentration of the verotoxin used was 7 µM in 4th and 5th round and 0.1 µM from 6th to 8th round of selection. The eluted mRNA was purified using RNA Clean and Concentrator ^{TM}-25. The selection cycle was repeated for eight rounds (Figure 4). For the specificity of the selected peptide aptamer, negative selection was done using bovine serum albumin (BSA) immobilized plates from 3rd to 8th round.

d. RT-PCR of isolated mRNA

The isolated and purified mRNA was mixed with primer Rev Primer-1 and RNase in a nuclease-free tube and incubated at 65 °C for 5 min. Again for 5 min the mixture was cooled immediately on ice for 2 min and the reaction mixture was prepared by combining with reverse transcriptase, pipetted gently and incubated at 50 °C for 1h and at 70 °C for 15 min. PCR was performed to amplify the reverse transcription products using Fwd Primer-1 and Rev Primer-1 giving rise to DNAs. NucAway™ spin columns were used for the rapid removal of unincorporated nucleotides and salts from the DNA product. The concentration and quality of the DNA required for the next cycle was verified by UV absorbance and electrophoresis using 1.5 % agarose gel. The purified dsDNA was used as a template for the next round of the selection cycle.

e. Cloning and sequencing

After 8th round of selection cloning was done. For the cloning, Zero Blunt® TOPO® PCR cloning kit was used. The resultant DNA, TOPO vector (PCR™-Blunt II-TOPO®) and salt solution were mixed at room temperature with low vortex then the mixture was incubated on ice for 15 min. The ligated product was transformed into *E. Coli* and culture was done in LB medium containing 50 µg/mL Kanamycin. From the culture plate, 96 colonies were picked and colony PCR was performed using Fwd Primer-2 and Rev Primer-3. The presence of target product was confirmed by gel electrophoresis. Thus obtained PCR products were treated with Exo-SAP and the sequences were checked. Sequencing result was analyzed using clustalw software for the repetition of colonies. The sequence matching was performed using the online software Basic Local Alignment Tool, BLAST.

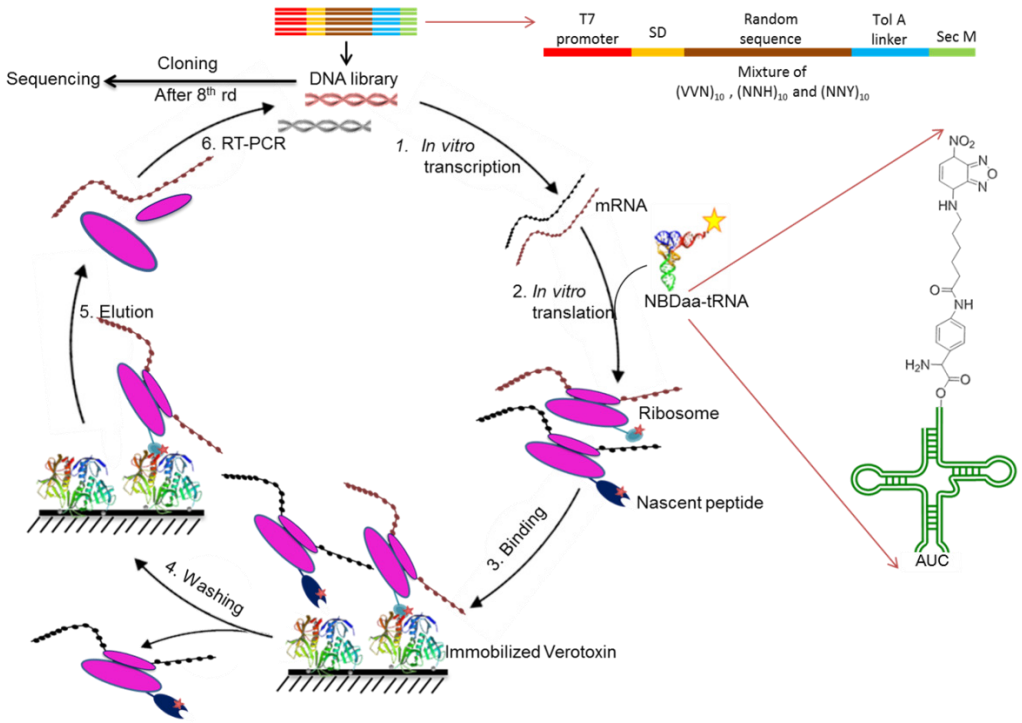

Figure 4: *In vitro* selection of verotoxin-binding peptide aptamer carrying NBDaa by ribosomal display.

2-2-2-3 Preparation of non-natural amino acid

First the preparation of NBD labeled amino acid (Figure 5) was carried out as previously reported[52]. NBD-Cl was mixed with caproic acid in equal molar ratio in the presence of three times the molar concentration of $NaHCO_3$. This mixture was stirred in MeOH at 0 °C for 30 min, then at room temperature (RT) for 2 hr and again at 50 °C for 2 hr. The reaction was cooled to RT and carefully acidified with 0.1 M HCl. The solid was filtered off, purified on silica, eluting with $CHCl_3$ to $CHCl_3$/MeOH (50:1) to yield NBD-Caproic acid. This NBD-Caproic acid was mixed with 1.3 times molar ratio EDC/HCl and 1.2 times molar ratio N-Hydroxysuccinimide then dissolved in CH_2Cl_2 and stirred at RT overnight. The solvent was evaporated and the residue was washed with brine, dried over anhydrous sodium sulfate and evaporated under reduced pressure

to give NBD-Caproic acid-NHS ester as orange solid. This product was directly used in the next step without purification.

To the solution of pyridine-HCl pH 5: DMF (1:1) equal molar concentration of NBD-Caproic acid-NHS ester and Fmoc-4-amino-L-phenylalanine added and the mixture was stirred at 37 °C overnight. The solvent was evaporated under reduced pressure and the crude residues was purified by flash chromatography on silica gel (CH_2Cl_2:CH_3OH, 100:1 to 50:1, v/v) to give rise to NBDaa (non-natural amino acid) as orange solid. 1H NMR (400 MHz, DMSO, Appendix 1, 2) δ(ppm): 12.7168 (br, 1H), 9.792 (s, 1H), 9.535 (s, 1H), 8.478 (d, *J*= 8.8 Hz, 1H), 8.864 (d, *J*=7.6 Hz, 2H), 7.687 (d, *J*= 8.4 Hz, 1H), 7.631 (t, *J*=8.4 Hz, 2H), 7.480 (d, *J*=8.8 Hz, 2H), 7.396 (q, *J*=6.4 Hz, 2H), 7.328~7.259 (m, 2H), 7.163 (d, *J*= 8.0 Hz, 2H), 6.396 (d, *J*= 9.2 Hz, 1H), 4.214~4.065 (m, 5H), 3.460 (br, 2H), 3.017 (dd, *J1*=4.4 Hz, *J2*= 14.0 Hz, 1H), 2.802 (dd, *J1*=9.8 Hz, *J2*= 13.6 Hz, 2H,), 2.298 (t, *J*= 7.6 Hz, 2H), 1.174~1.603 (m, 4H), 1.444~1.370 (m, 2H). 13C NMR (100 MHz, DMSO, Appendix 3) δ(ppm): 173.313, 170.918, 155.874, 145.125, 144.409, 144.138, 143.718, 143.685, 140.615, 137.916, 137.677, 132.385, 129.225, 127.562, 127.019, 125.249, 125.167, 120.501, 120.032, 118.797, 99.078, 65.573, 55.582, 46.520, 43.204, 36.224, 35.903, 27.410, 26.027, 24.793. The resultant product also confirmed by MALDI-TOF MS analysis. From MALDI-TOF MS, calculated mass (M+Na) 701.24 and found was 701.202 (Appendix 4).

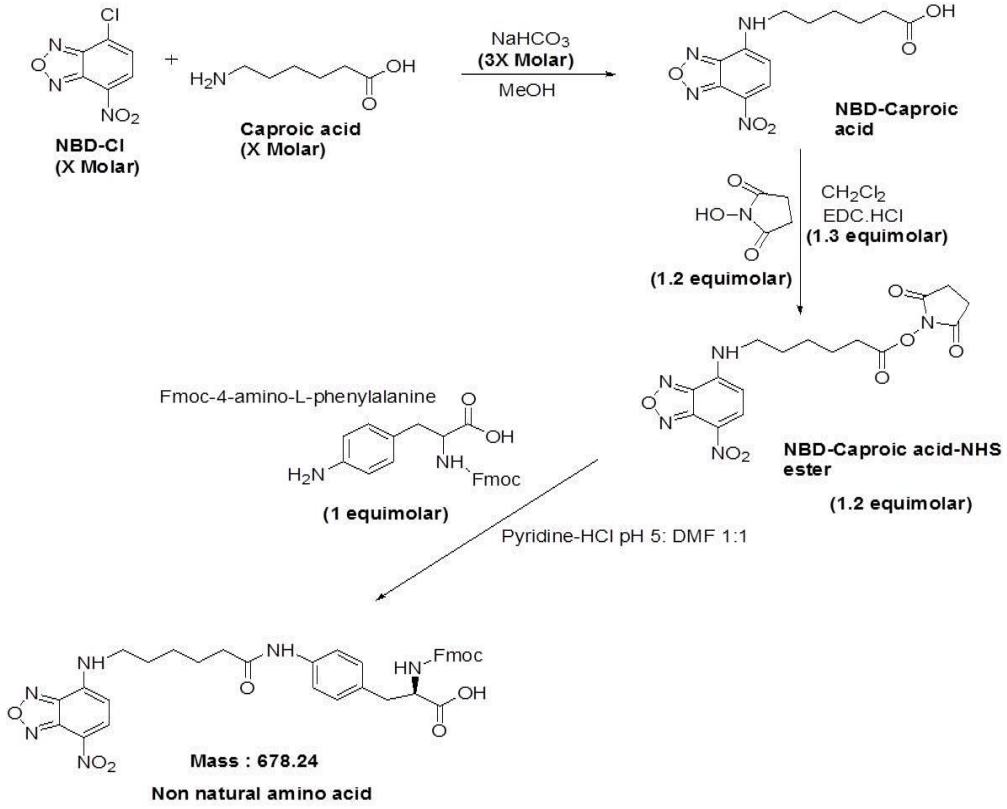

Figure 5: Synthesis of NBD labeled amino acid (NBDaa)

2-2-2-4 Peptide synthesis

For the NBD labelled peptides synthesis, microwave-assisted solid phase peptide synthesis was carried out using a single-mode manual microwave peptide synthesizer CEM Discover SPS (Matthews, USA). Both the coupling and de-protection steps were carried out according to the CEM experimental manual. All the peptides were synthesized on Rink Amide MBHA resin using 0.1 mmol scale. Fmoc protected resin (212.7 mg) was transferred into a reaction vessel and swollen in NMP for 30 min. Fmoc deprotection, 20 % piperidine in NMP was performed in two stages with an initial deprotection of 30 s followed by 3 min at 75 ± 5 °C. In the coupling steps, a 5 molar excess of the corresponding Fmoc-amino acid in combination with the standard

coupling cocktail N-ethyldiisopropylamine and 1-[bis(dimethylamino)methylene]-1H-1,2,3-triazolo[4,5-b]pyridinium 3-oxid hexafluorophosphate in NMP was used. The reaction mixture was irradiated in the microwave at 75 ± 5 °C for 5 min. For the coupling of histidine and cysteine were performed at 50 °C to reduce racemization of these amino acids, using an extended reaction time of 7 min. Similarly, coupling of a non-natural amino acid was carried out by applying our optimized condition (power 20 W, temperature 50 °C for 17.5 min). After completion of the peptide synthesis, the resin was de-protected and washed with NMP followed by chloroform and dried.

De-protection and cleavage of the peptide from the resin was achieved using trifluoroacetic acid (TFA) in the presence of scavengers (tri-isopropylsilane, m-cresol, thisoanisol, phenol and 1, 2-ethanedithiol), depending on the amino acids present and their protection groups. The cleavage mixture was filtered and treated with cold diethylether. The resulting precipitate was centrifuged, washed with diethylether then lyophilized for purification. The synthesized peptides were confirmed by MALDI-TOF mass analysis. The product was purified by reversed-phase HPLC using an Insertsil ODS-3 column (for 15 min with a linear gradient of 20–80 % acetonitrile in water containing 0.1 % TFA [v/v], at a flow rate of 1.0 mL/min and a column temperature of 25 °C). The synthesized peptides were purified using HPLC and again confirmed by MALDI-TOF-MS analysis (Appendix 5 and 6).

2-2-2-5 Solubility measurement

The synthesized peptides (5 μM) were dissolved in buffer (50 mM Tris-acetate, 150 mM NaCl, and 0.05 % Tween 20, pH 7) with 5 % DMSO and centrifuged at 9300 g for 5 min. After treatment, the absorbance was measured before and after centrifugation and visual inspection was performed after centrifugation to observe the sedimentation of the peptide.

2-2-2-6 Fluorescence measurement

Fluorescence measurements for all the peptides were performed on FP-6500 Spectrofluorometer (JASCO, Tokyo, Japan) at room temperature. First, the fluorescence of all the synthesized peptides and 4-chloro-7-nitro-2,1,3-benzoxadiazole (NBD-Cl) at the concentration of 1 μM was measured. Then to check the nature of interaction of peptides with protein, fluorescence intensity was checked by considering three various concentrations of verotoxin. The concentration of the peptide used was 1 μM and the concentrations of verotoxin used were 0, 1, 5 and 10 μM. After checking the fluorescence intensity nature, the concentration of verotoxin considered were 0-17.5 μM. Peptides and protein solutions were prepared in the buffer with 5% DMSO. The fluorescence spectra emission was set between 500 and 650 nm with an excitation at 470 nm. The changes in the fluorescence intensity with and without verotoxin were recorded. The experiments were performed in triplicates followed by the calculation of the mean and standard error. Finally, the points were plotted using GraphPad Prism 6 (GraphPad Software Inc., USA). To check the selectivity of the peptide aptamer, the titration of VT4 (1 μM) vs BSA (0-17.5μM) was carried out.

For the pH and ion effect on the performance of peptide aptamer (VT4) fluorescence intensity in different pH and ion concentration were measured. Here, the concentration of VT4 used was 1 μM and the concentrations of verotoxin used were 0-5.0 μM. The pH of the solution was varied from 4-10 and the ion concentration ranged between 150-1000 mM.

For the reversibility study of VT4 peptide aptamer towards verotoxin, fluorescence intensity of protein-peptide complex was measured at pH 7 and re-measured after changing the complex pH to 3.5. Similarly, the fluorescence intensity was measured taking protein-peptide complex pH 3.5 and changing to pH 7. For this analysis, concentration of VT4 used was 1 μM and the concentration of verotoxin used was 2.5 μM. The data analysis for pH effect and ion effect were done by plotting fluorescence intensity ratio against concentration of verotoxin using GraphPad Prism 6.

2-2-2-7 Dot blot analysis

This analysis was performed using polyvinylidene fluoride (PVF) membrane. First the blotting paper in blotting buffer and the required size PVF membrane were soaked in blotting buffer then in methanol for 20-30 sec respectively. The soaked membrane was placed on the soaked blotting paper. Then prepared protein samples (2 μL) were spotted onto the membranes and dried at room temperature. The membranes were then soaked in methanol and then in blotting buffer. Then the membrane was washed with TBST buffer for 3 times and then blocked for 30 min with blocking buffer. The membrane were then washed three times (5 min) with TBST and incubated with 10 μM VT4 peptide solution at room temperature for 1 hr. The membranes were washed three times (5 min) with TBST then the photo was captured using a Molecular Imager

FX (BioRad, USA). The peptide concentration used was 10 μM and the range of concentrations of protein used was 5-0.62 μM. For the comparison of verotoxin with other proteins the concentration of proteins used were 2 μM. The different proteins used for comparision were verotoxin, BSA, calmodulin, gelatin, IgG, β-Lactoglobulin and ovalbumin.

2-3 Results and Discussion

2-3-1 Construction of non-natural peptide libraries

In this study, I involved *in vitro*, ribosomal display technology using non-natural amino acid carrying tRNA suppressor strategy for incorporation of unnatural amino acids (Figure 6). Increase in the expression of amino acid would increase the diversity which on the other hand enables the detection of greatly enhanced ligands.

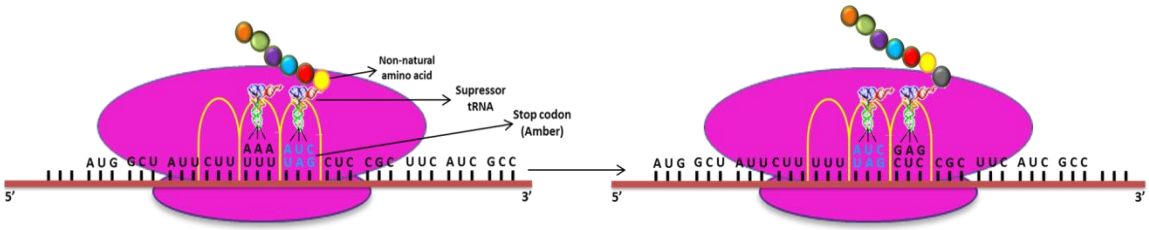

Figure 6: Introducing non- natural residues into ribosomal display libraries. *In vitro* nonsense suppression using a chemically aminoacylated suppressor tRNA to insert NBD labelled amino acid in ribosomal display libraries.

2-3-2 Cloning and peptide sequences

After the 8th round of selection, cloning was carried out and 90 peptide sequences were successfully found. Seventeen unique peptide sequences were originated after considering all the duplicate sequences. The sequence having the most frequency was MAIGVBFAYLCLGGLSG. Ten sequences were at least two repetitions followed by seven sequences with no repetition. Seven peptide sequences were selected based upon maximum frequency (Table 1) and synthesized by the solid phase method. Synthesized peptides were confirmed by MALDI-MS then purified using HPLC. The purified products were lyophilized and again confirmed by MALDI-TOF mass spectroscopy (Appendix 7-10).

Table 1 Selected sequences and synthesized peptides

Peptide Names	Clone repeat No.	Peptide sequences[a]	Molecular weight		Hydrophobic percentage[b]
			Calculated	Observed	
VT1	20	IGVBFAYLCLG	1492.7	1492.9	80
VT2	14	VVLBVSHRVLI	1571.9	1571.8	70
VT3	11	GVLBLYLVTRF	1617.9	1618.2	70
VT4	10	ILFBLRFIAFR	1733.0	1723.7	80
VT5	9	IFLBLLLSSSY	1614.8	1615.2	70
VT6	6	YFIBHAHLYFN	1761.8	1761.7	70
VT7	4	FSLBLTYFAVR	1653.9	1653.2	70

[a]B, NBD coupled phenylalanine

[b]Hydrophobic percentage calculated using the 'Peptide property calculator – LifeTein' online software excluding B, a non-natural amino acid.

The selected seven sequences were matched using BLAST with the reported verotoxin interacting sequences of the globotriaoside, GB_3 mimic peptide sequence[53] and GB_3 sequence[54] but none of them were found to have any similarity.

2-3-3 Solubility

Although the random sequence of DNA coding hydrophilic amino acids was employed as the selection process, the sequences of the selected peptides were surprisingly hydrophobic. The calculated hydrophobicity of selected peptides range from 70 to 80 %. During the selection, the sequences were inserted into longer peptide sequences and complex with the ribosome and mRNA and were soluble in the selection

buffer. However, the short peptides required 5% DMSO for solubilization in the buffer. VT1 and VT4 showed the highest solubility, whereas VT3 and VT6 showed precipitation (sedimentation) after centrifugation.

2-3-4 Fluorescence of the peptides

The fluorescence of the selected NBD-modified peptide aptamer and NBD-Cl were measured (Figure 7). Although NBD-Cl has no fluorescence, the incorporation of this compound into the peptide gave rise to fluorescence for all peptides. The maximum fluorescence intensity of peptides VT1, VT2, VT3, VT4, VT5, VT6 and VT7 were observed at 535, 540, 534, 531, 541, 539 and 537 nm, respectively. VT4 showed the highest fluorescence intensity and shortest emission wavelength among all the peptides. This phenomenon indicates that a hydrophobic environment was formed around the NBD in VT4 as this peptide has the highest hydrophobicity as well as showing high solubility.

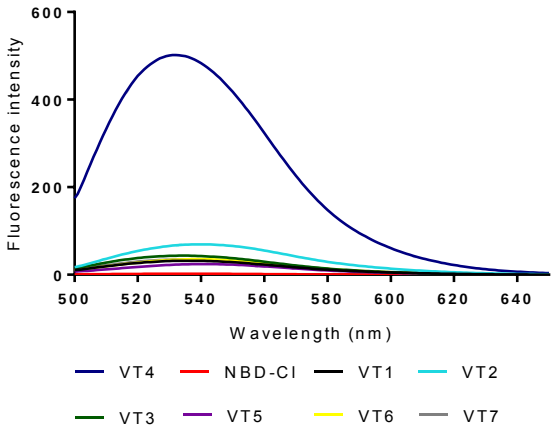

Figure 7: Fluorescence emission spectra from NBD-Cl and peptides at 1 µM concentration in the buffer with 5% DMSO. The excitation wavelength was 470 nm. The spectra were corrected by subtracting the baseline.

2-3-5 Interaction with verotoxin

The interaction of the selected NBD-modified peptide aptamer to verotoxin was tested by fluorescence titration measurement. Among the seven peptides, a fluorescent change was observed only for the VT4 peptide. 1 μM of peptides were allowed to equilibrate in the presence of 17.5 μM of verotoxin. The other peptides did not show any fluorescent change as the concentration of verotoxin was increased. The fluorescence of VT4 decreased by 78 % with increasing verotoxin concentration (Figure 8A). The aptamer bound to verotoxin with a dissociation constant (K_d) of 3.90 ± 1.6 μM. The dissociation constant was determined by fitting the data points on the one-phase exponential decay equation. In case of the selectivity analysis, the emission intensity and maxima of BSA was not changed by the addition of VT4, indicating that no interaction of VT4 with BSA (Figure 8B).

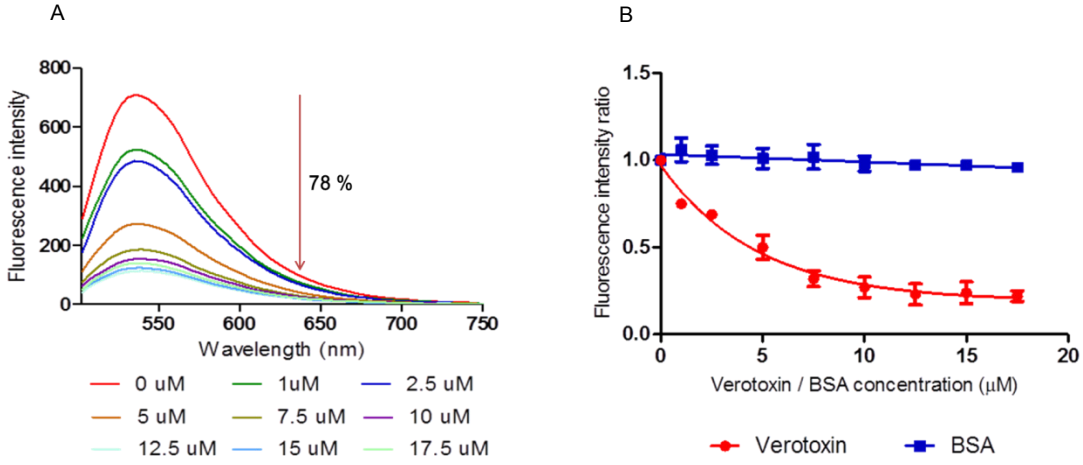

Figure 8: A. Fluorescence titration spectra of verotoxin with peptide VT4 at 1 μM concentration in the buffer with 5% DMSO. The excitation wavelength was 470 nm. The spectra were corrected by subtracting the baseline. B. Fluorescence titration of peptide VT4 with verotoxin and BSA. Data points and bars represent the means (± SEM) of three independent observations and the curve shows the best fit to a one–phase exponential decay equation, $n = 3$.

Previously calmodulin-dependent fluorogenic peptide aptamer using the same method was found[52]. In this case, the interaction between the fluorescence of the NBD-containing peptide aptamer increased following interaction with the target protein. In this research, as described above (Figure 7), a hydrophobic environment was formed around the NBD in VT4, thereby leading to an increase in the fluorescence as the concentration of peptide was increased. Conversely, in the presence of verotoxin, a decrease in fluorescence was seen, indicating the exposure of NBD to a hydrophilic environment owing to the interaction between the peptide and verotoxin as illustrated in Figure 9. As it is reported that the NBD is a hydrophobic dye and is highly environment sensitive which on binding with the hydrophobic domain enhances fluorescence intensity[52, 55] and when interacts with hydrophilic pocket reduces the fluorescence intensity[56]. There is the possibility of interaction of the peptide aptamer at the site 2 of verotoxin as this site facilitates the hydrogen bonding interaction as it is already reported that the interaction by the formation of hydrogen bonding decreases the fluorescence intensity[57].

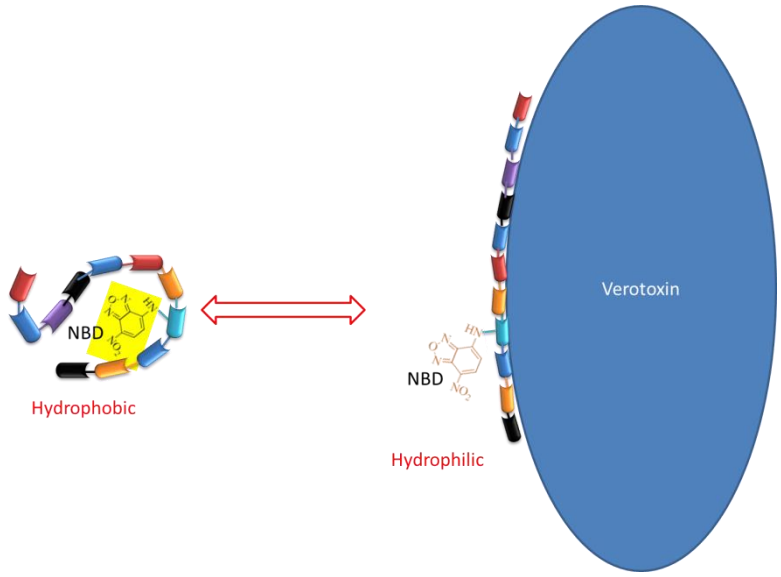

Figure 9: Illustration of NBD in VT4 in the absence and presence of verotoxin.

The ion effect was analyzed in the interaction with verotoxin. The fluorescence intensity of VT4 does not show any diverse on the specific interaction with the target (Figure 10). Changing the ion concentration from 150 to 1000 mM of NaCl has no effect on the interaction between the selected peptide and protein.

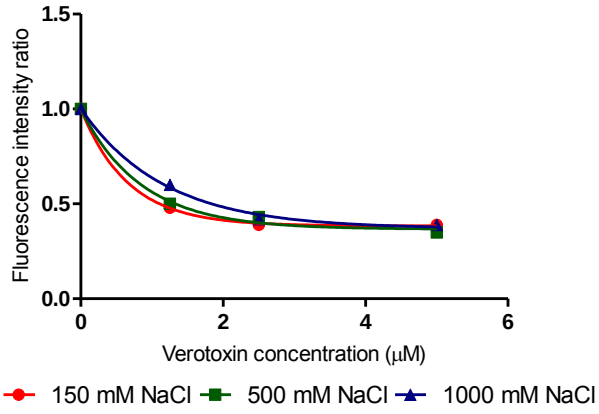

Figure 10: Fluorescence titration of peptide VT4 with verotoxin in different ion concentration (150 mM NaCl, 500 mM NaCl and 1000 mM NaCl). Data points represent the fluorescence intensity ratio at different concentration of VT4 vs verotoxin and the curve shows the best fit to a one–phase exponential decay equation.

The effect of pH was analyzed in the interaction with verotoxin (Figure 11) I can figure out that in low pH the interaction with the target is comparatively low than at high pH.

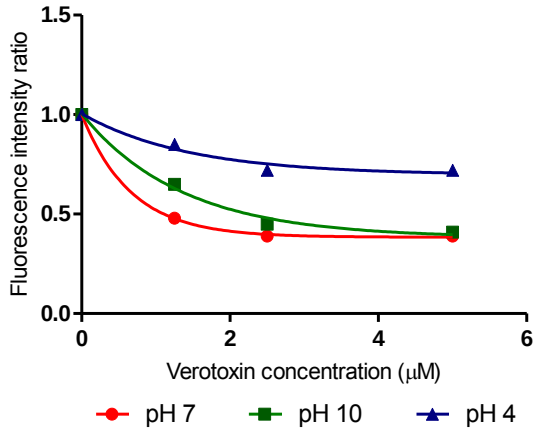

Figure 11: Fluorescence titration of peptide VT4 with verotoxin in different pH (4, 7 and 10). Data points represent the fluorescence intensity ratio at different pH of VT4 vs verotoxin and the curve shows the best fit to a one–phase exponential decay equation.

From the reversibility study carried out suggest that at pH 7 the aptamer has interaction with verotoxin but on decreasing the pH to 3.5 no change in interaction was seen on the other hand, there is no interaction at low pH 3.5 and on increasing the pH to 7 still the interaction with the protein doesn't take place thus shows no reversibility by altering the pH of solution from 7 to 3.5 and from 3.5 to 7 (Figure 12). The absence of reversibility might be due to the improper selection of the reversibility test method.

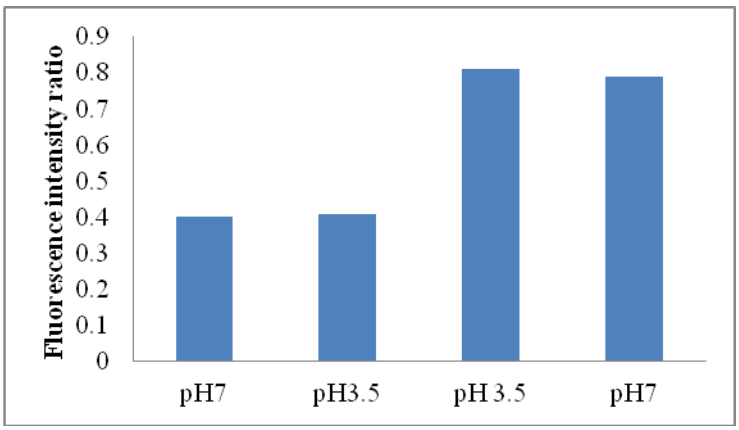

Figure 12: Reversibility study

2-3-6 Dot blot analysis

From the dot blot analysis, only spot of interaction of VT4 on verotoxin blotted region was seen (Figure 13A). Although no decrease of fluorescence was observed on the area blotted with BSA and ovalbumin in different concentration, the blotting of verotoxin significantly reduced the fluorescence. For more confirmation about the specificity, the peptide aptamer's performance was examined with other proteins (Figure 13B). From the figure, it is clear that VT4 specifically binds with target verotoxin and not with other proteins (BSA, calmodulin, gelatin, IgG, B-Lactoglobulin and ovalbumin). Thus, this result demonstrates that the peptide detects verotoxin selectively.

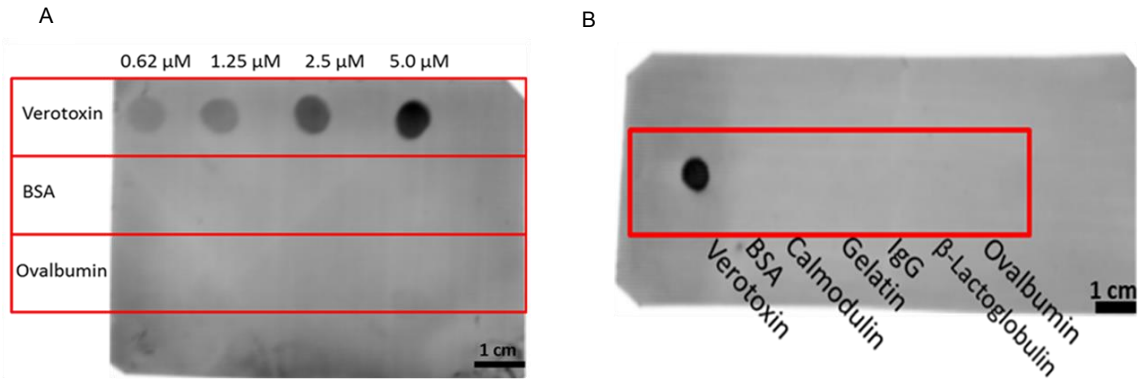

Figure 13: A. Fluorescence image of the VT4 peptide with verotoxin, BSA and ovalbumin blotted on a PVF membrane at different concentrations. B. Fluorescence image of the VT4 peptide with 2 µM concentration of various proteins blotted on a PVF membrane (scale bar, 1 cm).

2-4 Conclusion

A signaling peptide aptamer that showed a decrease in fluorescence upon binding verotoxin was successfully *in vitro* selected using ribosome display with a tRNA carrying an environment-sensitive fluorescent probe. This selected peptide by molecular evolutionary engineering technique can be used for the detection of verotoxin.

References

1. Borrebaeck CAK. Antibodies in diagnostics - from immunoassays to protein chips. *Immunol Today*, 21, 2000, pp 379-382.

2. Jhaveri S, et al. In vitro selection of signaling aptamers. *Nat Biotechnol*, 18, 2000, pp 1293-1297.

3. Nutiu R and Li Y. Structure-switching signaling aptamers. *J Am Chem Soc*, 125, 2003, pp 4771-4778.

4. Yang CJ, et al. Light-switching excimer probes for rapid protein monitoring in complex biological fluids. Proc Natl Acad Sci USA, 102, 2005, pp 17278-17283.

5. Paige JS, et al. Fluorescence imaging of cellular metabolites with RNA. *Science*, 335, 2012, pp 1194-1196.

6. Li Z, et al. In vitro selection of peptide aptamers with affinity to single-wall carbon nanotubes using a ribosome display. *Biotechnol Lett*, 35, 2013, pp 39-45.

7. Li Z, et al. In vitro selection of peptide aptamers using a ribosome display for a conducting polymer. *J Biosci Bioeng*, 117, 2014, pp 501-503.

8. Tada S, et al. Direct in vitro selection of titanium-binding epidermal growth factor. *Biomaterials*, 35, 2014, pp 3497-3503.

9. Ito Y and Tada S. Bio-orthogonal and combinatorial approaches for design of binding growth factors. *Biomaterials*, 34, 2013, pp 7565-7574.

10. Liu M, et al. In vitro selection of a photo-responsive peptide aptamer by ribosome display. *Chem Commun*, 48, 2012, pp 11871-11873.

11. Wang W, et al. Polypeptide aptamer selection using a stabilized ribosome display. *J Biosci Bioeng*, 112, 2011, pp 515-517.

12. Li S, et al. In vitro selection of mRNA display libraries containing an unnatural amino acid. *J Am Chem Soc*, 124, 2002, pp 9972-9973.

13. Muranaka N, et al. Four-base codon mediated mRNA display to construct peptide libraries that contain multiple nonnatural amino acids. *Nucleic Acids Res*, 34, 2006, pp 1-9.

14. Uzawa T, et al. Expansion of aptamer library from ‘‘natural soup’’ to ‘‘unnatural soup’’. *Chem Commun*, 49, 2013, pp 1786–1795.

15. 10.2210/pdb2xsc/pdb

16. Arya P, et al. α–galactose based neoglycopeptides. Inhibition of verotoxin binding to globotrisylceramide. *Bioorg. Med. Chem.*, 7, 1999, pp 2823-2833.

17. Lindberg A A, et al. Identification of the carbohydrate receptor for Shiga toxin produced by *Shigella dysenteriae* Type 1. *The journal of biological chemistry*, 262, 1987, pp 1779-1785.

18. Eiklid K. and Olsnes S. Interaction of Shigella Shigae cytotoxin with receptors on sensitive and insensitive cells. *J. Recept. Res.*, 1, 1980, pp 199-213.

19. MacKenzie CR, et al. Quantitative analysis of bacterial toxin affinity and specificity for glycolipid receptors by surface plasmon resonance. *The journal of biological chemistry*, 272, 1997, pp 5533-5538.

20. Ling H, et al. Structure of the Shiga-like toxin I B-pentamer complexed with an analodue of ita receptor Gb_3. *Biochemistry*, 37, 1998, pp 1777-1788.

21. Keusch GT, et al. Globotriaosylceramide, Gb_3, is an alternative functional receptor for Shiga-like toxin 2e. *infection and immunity*, 63, 1995, pp 1138-1141.

22. Shin IS, et al. Globotriaosylceramide (Gb_3) content in HeLa cells is correlated to Shiga toxin-induced cytotoxicity and Gb_3 synthase expression. *BMA reports*, 2009, pp 310-314.

23. Johannes, et al. Shiga toxin B-subunit as a vector for tumor diagnosis and drug delivery to Gb_3 expressing tumors. *US patent application publication*, 0243914A1, 2011, pp 1-13.

24. Calderwood SB, et al. Nucleotide sequence of the Shiga-like toxin genes of Escherichia coli. Proc. Natl. Acad. Sci., 84, 1987, pp 4364-4368.

25. Fraser M, et al. Crystal structure of the holotoxin from Shigella dysenteriae at 2.5°A resolution. Nat. Struct. Biol., 1, 1994, pp 59-64.

26. Ling H, et al. A mutant Shiga-like toxin IIe bound to its receptor Gb3: structure of a group II Shiga-like toxin with altered binding specificity. Structure, 8, 2000, pp 253-264.

27. Stein PE, et al. Crystal structure of the cell binding B oligomer of verotoxin-1 *E. coli*. *Nature*, 355, 1992, pp 748-750.

28. Soltyk AM, et al. A mutational analysis of the globotriaosylceramide-binding sites of verotoxin VT1. *The journal of biological chemistry*, 277, 2002, pp5351-5359.

29. Watanabe M, et al. Structural analysis of the interaction between Shiga toxin B subunits and linear polymers bearing clustered globotriose residues. *Infection and immunity*, 74, 2006, pp 1984-1988.

30. Pina DG, Et al. Shiga toxin B-subunit sequential binding to its natural receptor in lipid membranes. *Biochimica et Biophysica Acta*, 1768, 2007, pp 628-636.

31. Kitova EN, et al. Affinities of Shiga toxins 1 and 2 for univalent and oligovalent Pk-trisaccharide analogs measured by electrospray ionization mass spectrometry. *Glycobiology*, 17, 2007, pp 1127-1137.

32. Karve SS and Weiss AA. Glycolipid binding preferences of Shiga toxin variants. *PLOS one*, 9, 2014, pp 1-10.

33. St. Hilaire PM, et al. Interaction of the Shiga-like toxin type 1 B-subunit with its carbohydrate receptor. *Biochemistry*, 33, 1994, pp 14452-14463.

34. Gallegos KM, et al. Shiga toxin binding to glycolipids and glycans. *PLOS one*, 7, 2012, pp 1-10.

35. Kittell FB, et al. Characterization and inactivation of verotoxin 1 produced by *Escherichia coli* 0157:H7, *J. agric. Food. Chem.*, 39, 1991, pp 141-145.

36. Chae C. Shiga toxin, shiga-like toxin and verotoxin. *Korean vet res*, 33, 1993, pp 773-779.

37. Hattum H, et al. Functional assay for shiga-like toxin via detection by antibody capture and multivalent galabiose binding. *Bioorganic & medicinal chemistry letters*, 22, 2012, pp 7448-7450.

38. Muniesa M, et al. Shiga toxin-producing *Escherichia coli* 0104:H4: a new challenge for microbiology. *Applied and environmental microbiology*, 78, 2012, pp 4065-4073.

39. Michino H, et al. Massive outbreak of *Escherichia coli* 0157:H7 infection in school children in Sakai city, Japan, associated with consumption of white radish sprouts. *Am J Epidemiol*, 150, 1999, pp 787-796.

40. Park CH, et al. Evaluation of the Duopath verotoxin test for detection of Shiga toxins in cultures of human stools. *J. Clin. Microbiol.*, 41, 2003, pp 2650-2653.

41. Kai E, et al. Detection of PCR products of *Escherichia coli* 0157:H7 in human stool samples using surface plasmon resonance (SPR). *FEMS Immunology and medical microbiology*, 29, 2000, pp283-288.

42. Slinchenko O, et al. Imprinted polymer layer for recognizing double-stranded DNA. *Biosensors and bioelectronics*, 20, 2004, pp 1091-1097.

43. Yamazaki et al. A rapid bioluminescent enzyme immunoassay (BLEIA) for the detection of Shiga toxin types 1 and 2. *Microbiology and immunology*. 45, 2001, pp 621-628.

44. Miyra Y, et al. Peptides binding to a Gb3 mimic selected from a phage library. *Biochimica et Biophysica Acta*, 1673, 2004, pp 131-138.

45. Kanda V, et al. Surface plasmon resonance imaging measurements of the inhibition of Shiga-like toxin by synthetic multivalent inhibitors. *Anal. Chem.*, 77, 2005, pp 7497-7504.

46. Challa S, et al. Selective evolution of ligands by exponential enrichment to identify RNA aptamers against Shiga toxins. *Journal of nucleic acids*, 2014, pp 1-8.

47. Tzipori S, et al. Antibody therapy in the management of Shiga toxin-induced hemolytic uremic syndrome. *Clinical microbiology reviews*, 17, 2004, pp 926-941.

48. Goldwater PN and Bettelheim KA. Treatment of enterohemorrhagic *Escherichia coli* (EHEC) infection and hemolytic uremic syndrome (HUS). *BMC medicine*, 10, 2012, pp 1-8.

49. Rowe PC, et al. A phase II randomized controlled trial of Synsorb-Pk for the prevention of hemolytic uremic syndrome in children with verotoxin-producing *E. coli* (VTEC) gastroenteritis. *Pediatric research*, 41, 1997, pp 283.

50. Phase III randomized study of Synsorb Pk in children with *E. coli* associated hemolytic uremic syndrome. *Clinical trials.gov*. (https://clinicaltrials.gov/ct2/show/NCT00004465)

51. Yamazaki M, et al. A rapid bioluminescent enzyme immunoassay (BLEIA) for the detection of Shiga Toxin types 1 and 2. *Microbiol Immunol*, 45, 2001, pp 621-628.

52. Wang W, et al. A fluorogenic peptide probe developed by in vitro selection using tRNA carrying a fluorogenic amino acid. *Chem Commun*, 50, 2014, pp2962-2964.

53. Yamada Y, et al. Design of multifunctional peptides expressing both antimicrobial activity and shiga toxin neutralization activity. *Bioorg Med Chem*, 14, 2006, pp 77-82.

54. Keusch JJ, et al. Cloning of GB_3 synthase, the key enzyme in globo-series glycosphingolipid synthesis, predicts a family of α1, 4-glycosyltransferases conserved in plants, insects and mammals. *J Biol Chem*, 275, 2000, pp 25315-25321.

55. Marvin JS, et al. The rational design of allosteric interactions in a monomeric protein and its applications to the construction of biosensors. *Proc. Natl. Acad. Sci. USA*, 94, 1997, pp 4366-4371.

56. Gilardi G., et al. Engineering the maltose binding protein for reagentless fluorescence sensing. *Anal. Chem.*, 66, 1994, pp 3840-3847.

57. Jespers L., et al. Selection of optical biosensors from chemisynthetic antibody libraries. *Protein engineering, design & selection*, 17, 2004, pp 709-713.

CHAPTER 3

INTERACTIONS OF IN VITRO SELECTED FLUOROGENIC PEPTIDE APTAMERS WITH CALMODULIN

3-1 Introduction

Aptamers are functional nucleic acids or peptides isolated from very large random sequence libraries by *in vitro* selection based on the affinity to the desired specific target[1-2]. The selection of proteins and peptides with desired functions were achieved first using phage display[3] and the subsequent *in vitro* translation system including ribosome and mRNA display[4-6]. Evolutionary molecular biology has opened a new window to evolve artificial aptamers from a library including non-natural amino acid with the implementation of ribosome and mRNA display selection technique[7-9]. The incorporated number of non-natural components in the selection library is increasing and I call this transitional period of selection library moving from "natural soup" to "unnatural soup"[10].

The kinds of unnatural component incorporated in the selection library have increased. For example, photo-isomerizable, fluorogenic or inhibitor has been successfully incorporated into the aptamers. These functional groups added new artificial functions to the aptamers which inherently has molecular recognition function. In particular, fluorescence signaling is one of the promising functions for analytical application, because the technology realizes universal analysis of arbitrary targets without bound/free separation.

Our previous study selected fluorogenic peptides that bind to calmodulin (CaM) by combination of ribosome display and bioorthogonally prepared tRNA [11-14]. These peptides has the incorporation of a hydrophobic indicator, 7-nitro-2,1,3-benzoxadiazole (NBD), that emits fluorescence in hydrophobic environment. However, the site specific interactions between selected aptamers and the same target have not been structurally investigated in detail. Thus, in this study, I chose

several major populations of selected aptamer sequences to check their site specific interaction. I characterized the peptides, confirmed their binding behaviors and studied about the residues involved in binding using various techniques such as fluorescence, surface plasmon resonance and nuclear magnetic resonance measurements.

The target was calmodulin which is a Calcium Modulated protein. It is a small and important messenger protein having only 148 amino acids that activates its numerous target proteins[15-19]. This protein is a multi-functional receptor in animal and plant cells regulating many important physiological functions[20-22]. The crystal structure of CaM is an unusual dumbbell shape consisting of a long central helix and two globular homologus domains (N and C) connected by a flexible central linker each containing two helix calcium binding motifs known as EF hands (Figure 1). In these domains, binding of Ca^{2+} to CaM induces conformational changes that exposes hydrophobic amino acid residues on the surface of both lobes, creating hydrophobic patchs[12, 23-27]. These hydrophobic sites can bind with hydrophobic drugs that inhibit CaM activity, inhibitory ligands like CaM antagonist, Ca^{2+} ions antagonists, CaM binding proteins and various hydrophobic fluorescent probe molecules[28]. By binding to more than 100 cellular proteins, CaM transduces intracellular (Ca^{2+}) changes into numerous cellular events[29]. It is an essential regulator of intracellular processes in response to extracellular stimuli mediated by the increase in calcium ion concentration[30-35]. Identification of many Ca^{2+}-CaM binding proteins has been done. CaM plays a vital role in a wide range of cellular Ca^{2+} dependent signaling pathways through various enzymes such as Ca^{2+}-CaM dependent protein kinase, CaMKI, CaMKII and CaMKIII[27, 31-32, 36-37], cyclic nucleotide phosphodiesterase[38-41], NADPH

oxidase[42], ATPase[43-44], adenyl cyclase[45-47], myosin light-chain kinase[46, 48], inositol triphosphate kinase and nicotinamide adenine dinucleotide kinase[49].

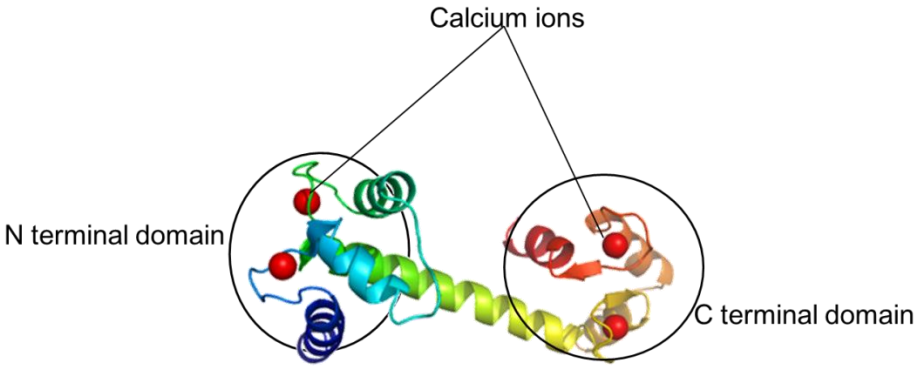

Figure 1: Calmodulin with calcium ions (PDB ID: 3cln)

Previously, phage display has been used to isolate CaM binding peptide library[38, 50]. The selected CaM binding sequences could not be sufficiently correlated with naturally occurring proteins[51]. The next method widely used to isolate CaM binding proteins and study protein–protein interaction was yeast two-hybrid analysis. However, only limited number of CaM-binding proteins were reported due to the limited library size caused by the use of living cells. To overcome these limitations, mRNA display and ribosomal display can be used. mRNA display has been used as it circumvents the difficulties associated with phage and yeast two-hybrid display as well provides a powerful means for reading and amplifying a protein sequence after been selected from large libraries, 10^{12}-10^{13} [52].

However, CaM-binding peptide aptamers were selected carrying fluorogenic dye 7-Nitro-2,1,3-benzoxadiazole (NBD, a hydrophobic indicator that changes fluorescence intensity in response to surrounding environment) from random library using ribosome display. Among the selected peptide aptamers, C5 (YWDKIKDXIGG;

X: NBD coupled phenylalanine) was found to have a strong binding affinity (K_d= 850 nM) with the C domain of CaM[11-12].

Depending on the high frequency among the selected peptides, four peptides were synthesized with 5 fixed residues (MAMQA) to the N-terminal of the peptide sequences which comes from the restriction enzyme site during the selection (Table 1). For the binding, the peptides must be fold correctively into its three-dimensional structure thus the elongation of the peptide may help for this. To synthesize the selected peptides by solid phase peptide synthesis (SPPS), first NBD linked aminophenylalanine was prepared and used as non-natural amino acid.

Table 1 Selected peptide sequences with 5 fixed residues on N terminal

Synthetic peptides	Clone repeat no.	Sequence with 5 fixed residues on N terminal
MA4	5	MAMQAVVNXVMTQQAG
MB4	9	MAMQASNIXYANKLRR
MC5	4	MAMQAYWDKIKDXIGG
MD9	2	MAMQADMASLVAXVMD

X, NBD coupled phenylalanine

3-2 Materials and Methods

3-2-1 Materials

Calmodulin from bovine testes (Sigma Aldrich, USA).

2-Amino-2-Hydorxy methyl-1,3-propanediol (Wako Pure Chem. Ind. Ltd., Japan)

Potassium chloride (Wako Pure Chem. Ind. Ltd., Japan)

Calcium chloride dehydrate (Wako Pure Chem. Ind. Ltd., Japan)

Magnesium acetate tetrahydrate, 99.9% (Wako Pure Chem. Ind. Ltd., Japan)

Tween® 20, Molecular biology grade (Promega, USA)

Dimethyl sulfoxide (Wako Pure Chem. Ind. Ltd., Japan)

Phosphate Buffered Salts, Dulbecco's formula (modified) without magnesium and calcium (Takara, Japan)

Sodium acetate, anhydrous (Wako Pure Chem. Ind. Ltd., Japan)

Sodium hydroxide (Wako Pure Chem. Ind. Ltd., Japan)

O,O'-Bis (2-aminoethyl) ethyleneglycol-N,N,N',N'-tetraacetic acid (Dojindo, Japan)

Acetic acid (Wako Pure Chem. Ind. Ltd., Japan)

Series S Sensor chip CM5 (GE, Sweden)

N-hydroxysuccinimide (Tokyo, Japan)

1-Ethyl-3-(3- dimethylaminopropyl) carbodimide, hydrochloride (Dojindo, Japan)

2-Aminoethanol (Monoethanolamine) (Wako Pure Chem. Ind. Ltd., Japan)

Buffer (50 mM Tris-acetate, 150 mM KCl, 50 mM $Mg(OAc)_2$, 5% DMSO, pH 7.0 with 5 mM $CaCl_2$)

3-2-2 Methods

3-2-2-1 Solubility

The synthesized peptides were dissolved in buffer (50 mM Tris-acetate, 150 mM Potassium chloride, 50 mM Magnesium acetate, 5 % DMSO) pH 7.0 with 5 mM calcium chloride. Prepared 5 μM solution was centrifuge at 14000g for 20 min and absorbance was measured before and after centrifuge.

3-2-2-2 Fluorescence measurement

The relative fluorescence intensity changes (RFIC) was measured for all peptides with various concentration of CaM in presence of Ca^{2+}. The calculated RFIC were plotted using Graph Pad Prism 5 (Graph Pad Software, Inc., USA) and the dissociation constant (K_d) values were estimated by non-linear regression analysis of emission intensities at 535 nm. Excitation wavelength used was 488nm

3-2-2-3 Surface Plasmon Resonance (SPR) measurement

SPR, a more reckonable analysis was carried out to find the dissociation constant (K_d) values. The measurements were performed on a Biacore T100 instrument with a CM5 sensor chip (GE Healthcare Bio-Science, Sweden). First the pH scouting was done to find the optimal pH condition for immobilizing the ligand, CaM. This is done by testing ligand pre-concentration at a range of pH values more than pH 3.5 and less than isoelectric point (pI) of the protein. In this, the initial electrostatic attraction of CaM to the CM5 sensor Chip surface was best performed at a pH lower than its pI i.e. 3.9-4.3[59-61] and higher than pH 3.5, so that the sensor chip surface and the protein carry

opposite net charges. Thus, CaM was endeavored to immobilize to sensor chip surface in the range of 3.5 to 4.3. CaM, 50 µg/mL was immobilized on the sensor chip using pH 3.7 and pH 4.0 of 10 mM sodium acetate without Ca^{2+} and CaM was also tried to immobilize with pH 3.7 of 10 mM sodium acetate with Ca^{2+}. Then injection of 368 µL of CaM (50 µg/mL) at a flow rate of 10 µL/ min at 25 °C was done to immobilize CaM on the chip surface with amine coupling at best pH. After the immobilization of CaM on the sensor surface, affinity analysis were carried out for peptides MB4, MC5 and MD9. All the experiments were performed at 25 °C with a constant flow of 30 µL/min. For the affinity analysis, various concentrations of MB4 (0, 19.53, 39.06, 312.50, 1250, 2500 and 5000 nM); MC5 (0, 9.76, 19.53, 39.06, 78.12, 156.25, 312.50, 625, 1250, 2500 and 5000 nM) and MD9 (0, 19.53, 39.06, 156.25, 625, 1250, 2500, 5000 and 10000 nM) peptide solutions in buffer with 0.05 % surfactant Tween® 20 and 5 mM calcium chloride were injected over the sensor chip containing the immobilized CaM. The sensor chip was regenerated by injection of 50 mM EGTA (pH 8.0) for 30 sec, followed by buffer with 0.05 % surfactant Tween® 20 and 5 mM calcium chloride for 5 min to stabilize the baseline. This measurement was carried out in the presence of calcium ions only. All of the binding curves were collected by subtraction of the curve for a reference flow cell and fitted to a steady state affinity model using Biacore T100 Evaluation Software (version 2.0.3).

3-2-2-4 Nuclear Magnetic Resonance (NMR) measurement

3-2-2-4-1 *Observation of CaM-peptide aptamers by NMR*

NMR experiments for investigating the interaction of human CaM with MB4, MC5 and MD9 peptide apramers were performed in a triple-resonance CRYOPROBE

fitted with a Z-axis pulsed field gradient coil, using a 600 MHz Bruker Advance spectrometer at 298 K. All NMR spectra were processed on LINUX-PCs using the Azara 2.8 suite of software, Boucher[61], then visualized and analyzed on LINUX-PCs using the CcpNmr Analysis 2.2.1 software[62].

For the NMR titration experiments of ^{15}N-labelled human CaM with MB4, MC5 and MD9 peptide aptamers, a series of 2D ^{1}H-^{15}N HSQC spectra were measured on ^{15}N-labelled CaM (0.1 mM) at various protein: peptide ratios in order to monitor gradual changes in the chemical shifts or intensity of ^{1}H-^{15}N correlation cross-peaks of CaM. ^{15}N-labelled human CaM sample was purified using the protocols presented previously[63]. ^{15}N-labelled CaM was dissolved in 50 mM Tris. HCl buffer (pH 7.5) containing 120 mM NaCl and 2.5 mM $CaCl_2$ and 10 % $^{2}H_2O$. 2D ^{1}H-^{15}N HSQC spectra were acquired with 8 transients and a total of 2048 (t2, $^{1}H^{N}$) $\times$256 (t1, ^{15}N) complex points. Initially, a reference spectrum was recorded in the absence of peptides. Then the sample was taken out of the NMR tube and mixed with a 20 mM peptide solution to achieve a protein: peptide molar ratio of 1:0.5, prior to the next measurement. More peptide solution was added incrementally to measure ^{1}H-^{15}N HSQC spectra at protein: peptide molar ratios of 1:1, 1:2 and 1:3. The concentration of the protein was not adjusted after each titration point due to the small volume of the peptide solution that was added.

Backbone $^{1}H^{N}$, ^{15}N, $^{13}C^{\alpha}$, $^{13}C^{'}$, and side-chain $^{13}C^{\beta}$ resonance assignments were performed on ^{13}C/^{15}N-labelled human CaM (0.1 mM for MD9 and 0.2 mM for MB4 and MC5) dissolved in 50 mM Tris. HCl buffer (pH 7.5) containing 120 mM NaCl and 2.5 mM $CaCl_2$ and 10 % $^{2}H_2O$ in the presence of 0.3 mM MD9 peptide aptamer and 0.6 mM MB4 and MC5 peptide. Four 3D triple-resonance NMR spectra, CBCA (CO)NH,

CBCANH, HNCO and HN(CA)CO were measured. To reduce the experimental time, a nonlinear sampling method[64-68] was utilised for the indirectly observed ^{15}N and ^{13}C dimensions. Approximately 1/8 of the points were selected in a pseudo-random fashion from the conventional regularly spaced grid of t1, t2 points. For the acquisition dimension ($^{1}H^{N}$) of 3D experiments, 1024 complex points were measured. The two-dimensional maximum entropy method[69] was used for processing of nonlinearly sampled ^{13}C and ^{15}N dimensions with improved resolution. Backbone resonance assignment of human CaM on its own under this experimental condition was also performed with essentially identical NMR protocols.

3-3 Results and Discussion

Selected aptamers MC5, MD9, and MB4 were compared with the naturally existing CaM binding proteins in plants[70] and in human[71-73] using the BLAST. Aptamers MC5 and MD9 did not show any similarity with CaM binding protein but, MB4 was found to have 25% similarity with the sequence of multi drug resistant protein[74], which is one of the CaM binding protein in human when. This result demonstrates that the *in vitro* selected peptide has the similarity to the protein sequence which is naturally evolved.

3-3-1 Solubility

MB4, MC5 and MD9 were found to be soluble in buffer with 5 mM calcium chloride. These three peptides were preceded for further experiments whereas peptide MA4 was found insoluble in buffer as well in 100% DMSO thus was not proceeded further. On the other hand, enhancement of solubility on peptide B4, C5 and D9 were seen on addition of 'MAMQA'. This is due to the presence of methionine and glutamine in the added fixed residue which has the ability to participate in hydrogen bonding[75].

3-3-2 Fluorescence measurement

The fluorescence of the three peptides (MB4, MC5 and MD9) in the presence of calcium ions were measured (Figure 6). As the fluorescence spectrum is very sensitive to the environment around this dye, this environment sensitive quality of NBD dye helps to know the effect of increase or decrease in fluorescent intensities on interaction. Peptides with five fixed residues were titrated with various concentrations of CaM. In the presence of Ca^{2+}, the fluorescent signal of MB4 peptide increased significantly up to 16 fold with a concomitant increase in CaM concentration to 10 μM

(Figure 6A). In case of MC5 and MD9, the increase in fluorescence intensity was by 3 and 3.5 folds respectively (Figure 6B and 6C).

The increase in fluorescence intensity suggests that the peptides bind in the hydrophobic area of CaM which is exposed on the availability of calcium ions. The increase in the fluorescence intensity on addition of CaM with the peptide is the clear indication of the capture of peptide in the hydrophobic lobes of CaM.

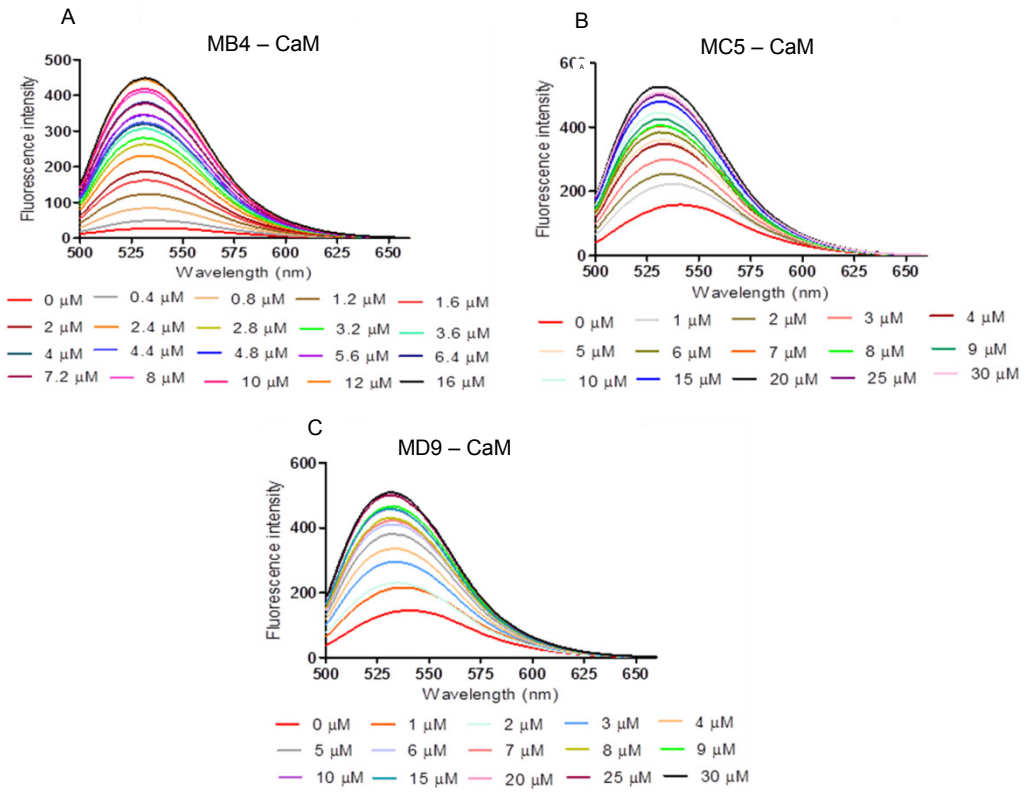

Figure 6: Fluorescence emission spectra from peptides MB4 (2 µM), MC5 (5 µM) and MD9 (5 µM) increased on addition of CaM concentration in the presence of Ca^{2+}. The excitation wavelength was 488 nm. The spectra were corrected by subtracting the base line.

From the change in fluorescence spectrum, the relative fluorescence intensity changes (RFIC) of peptide with CaM were calculated at maximum emission wavelength

535 nm. The fluorescence intensities of B4 did not showed any saturation upon the increase of calmodulin concentration up to 20 folds in the presence of calcium ion[12] but interestingly on addition of 'MAMQA' on B4, the saturation point was observed just by adding 5 fold excess CaM (Figure 7A).

Similarly, in case of peptide MC5 and MD9, fluorescence intensity was found to be increased on increasing the concentration of CaM till 15 μM indicating the binding of these peptides with the protein (Figure 7B and 7C). On the other hand without Ca^{2+}, the peptides scarcely bound to CaM (Figure 7). Thus the peptide interacts with CaM in a Ca^{2+} dependent manner. The RFIC of peptide with CaM was considered at maximum emission wavelength 535 nm in the presence of 5mM calcium chloride. Thus, the dissociation constant (K_d) between peptide and CaM were estimated maximum emission (Table 2).

Table 2 Peptides with dissociation constant values from Fluorescence

Synthetic peptides	Dissociation constant, K_d (μM)
MB4	2.2 ± 0.25
MC5	5.7 ± 0.22
MD9	4.8 ± 0.28

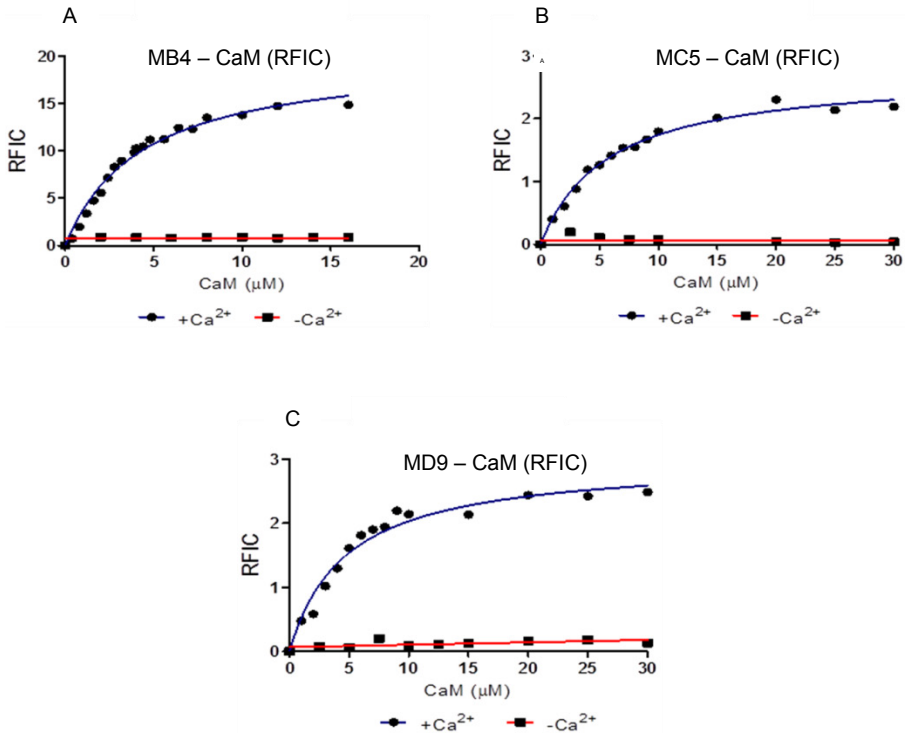

Figure 7: Data points in blue line represents the relative fluorescence intensity change (RFIC) of Ca^{2+} bound CaM at different concentrations and the curve shows the best fit to non-linear regression analysis of emission intensities at 535 nm. The red line containing data points indicates the RFIC in the absence of Ca^{2+} bound CaM.

3-3-3 SPR measurement

For the ligand immobilization pH scouting was done in three different pH conditions (pH 3.7, pH 4.0 and pH 3.7 in presence of calcium ions). Among the three condition, better curve was seen at pH 3.7 denoted by the red line (Figure 8). Since the CM5 sensor chip carries negative charge and below the pI the protein caries the positive charge resulting in the optimal condition for CaM immobilization.

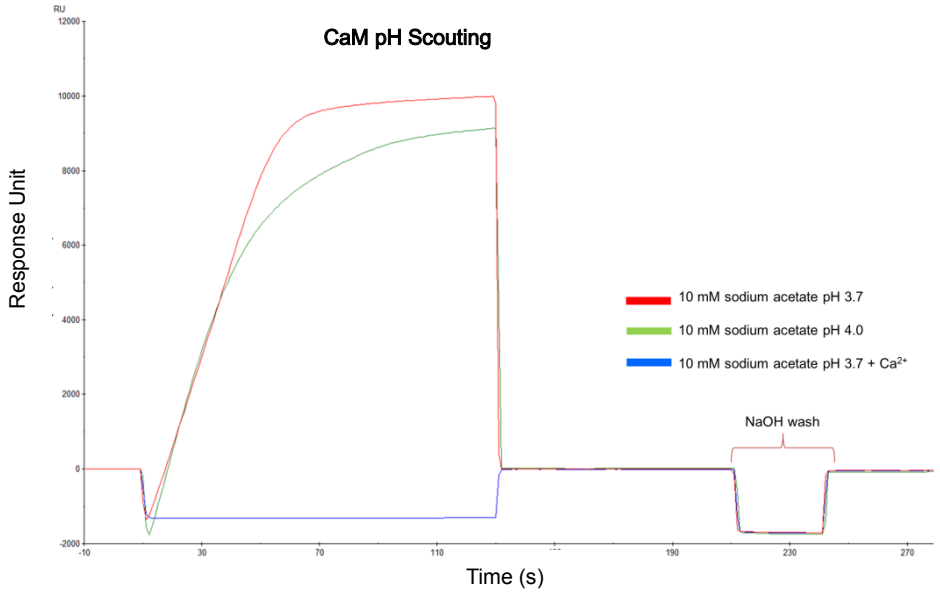

Figure 8: Senserogram showing the effect of pH on preconcentration of CaM on the CM5 chip surface. Red shows the scouting for optimal electrostatic preconcentration at pH 3.7, green line is the measure at pH 4.0 and blue line is at pH 3.7 with calcium ions.

After the optimal pH condition (pH scouting), ligand was immobilized by amine coupling. The calculated theoretical response unit was in the range of 304-1523 and the practical response unit on immobilizing protein concentration of 50 µg/mL was found to be 458, which lies in the range (Figure 9).

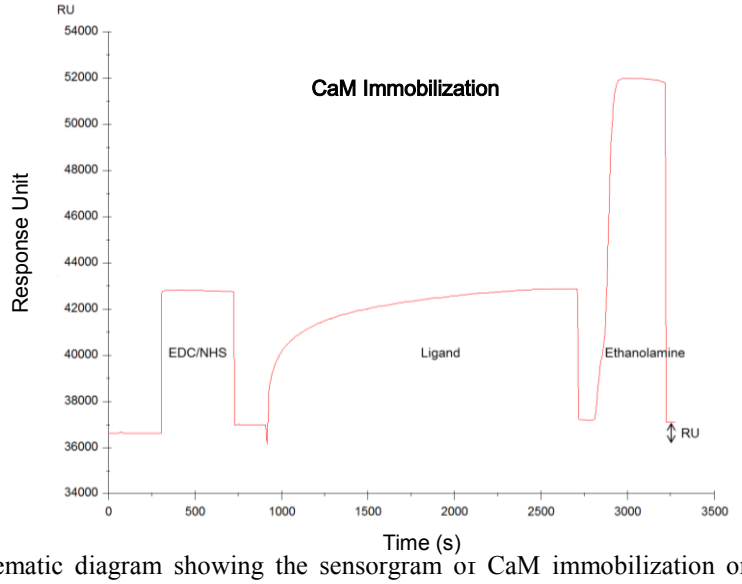

Figure 9: Schematic diagram showing the sensorgram of CaM immobilization on CM5 chip surface using amine coupling.

SPR analysis contributed the accurate and direct picture of binding of signaling peptide aptamers (MB4, MC5 and MD9) on immobilized CaM in the presence of Ca^{2+} (Figure 10). The interactions were Ca^{2+} dependent since 50 mM EGTA readily reverse the interaction. Determination of affinity analysis for peptides MB4, MC5 and MD9 by steady state affinity model (a model for 1:1 binding at two independent ligand, CaM sites) with dissociation constant values (Table 3).

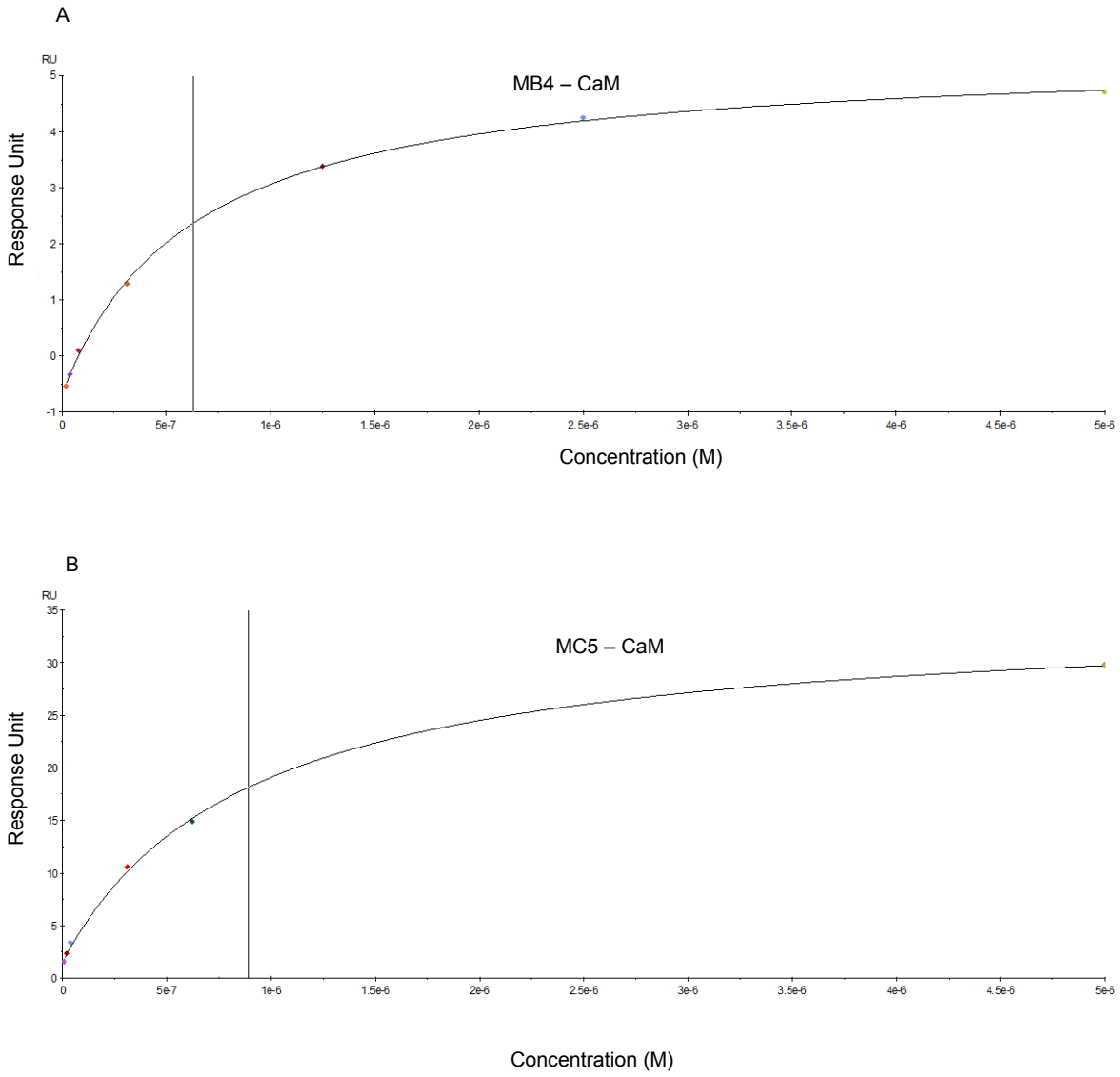

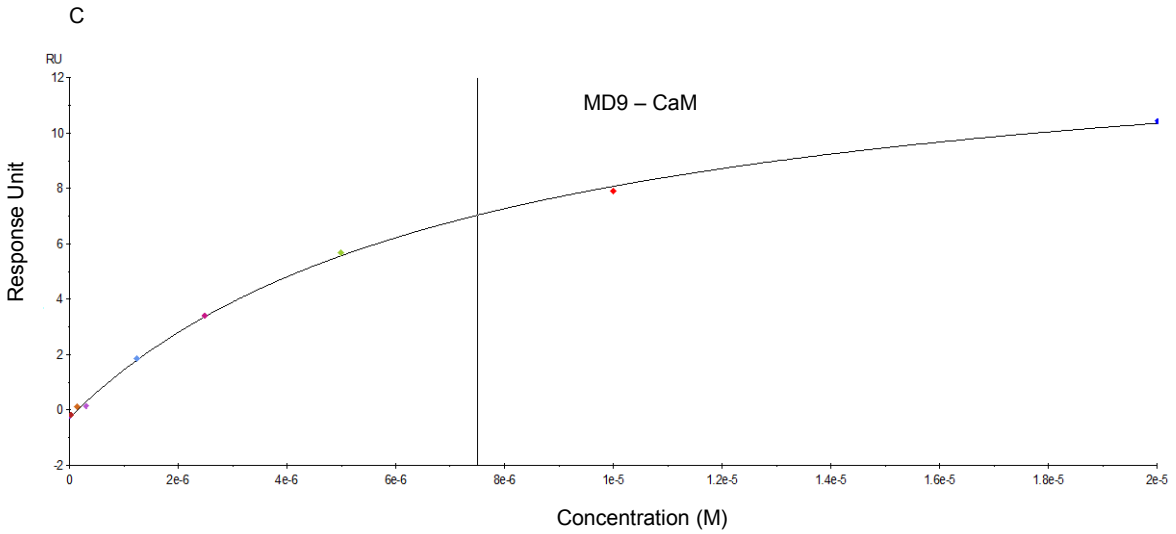

Figure 10: Fitting plots of response values against the concentration of peptides in steady state affinity model. Solid vertical line denotes the dissociation constants (K_d) value. In the figure, the vertical line in A shows the K_d for MB5 to be 0.6 ± 0.02 µM; the line in B represents K_d of MC5 to be 0.9 ± 0.05 µM and the final C shows the K_d for MD9 to be 7.5 ± 0.37 µM.

Table 3 Peptides with binding constant values from SPR

Synthetic peptides	Dissociation constant, K_d (µM)
MB4	0.6 ± 0.02
MC5	0.9 ± 0.05
MD9	7.5 ± 0.37

In case of peptide B4 and D9, binding with CaM was observed only after addition of fixed residue 'MAMQA'. This clarifies that other sequences in the full length displayed on ribosome affected the binding of peptide with CaM. Peptide MC5 bind with high affinity and the addition of fixed residue did not show the significant

change in binding affinity.

3-3-4 NMR measurement

The detail investigation of the binding mechanism of peptide aptamers MB4, MC5 and MD9 with CaM were characterized by a series of stepwise, multipoint NMR titration experiments (Figure 11) by employing ^{15}N-labelled human CaM (in collaboration with Pro. Ito, TMU). To monitor the ^{1}H-^{15}N correlation cross-peaks, 2D ^{1}H-^{15}N HSQC spectra were measured first in the absence of peptides and then at each titration point, aiming at identifying the binding interface on CaM.

In case of the NMR titration experiment of ^{15}N-labeled CaM with MB4 peptide, addition of MB4 peptide affected large numbers of CaM resonances. I observed the disappearance and emergence of signals, indicating that the timescale of the binding of CaM protein with MB4 peptide was a slow exchange. The disappearing and emerging of cross-peaks were initially observed upon the first point of titration (protein: peptide molar ratio of 1:0.5). On gradually increase of MB4 peptide concentration to saturate CaM protein to 0.3 mM (protein: peptide molar ratio of 1:3), large number of precipitates were observed and change in chemical shift of CaM protein was not saturated. Therefore, CaM protein and MB4 peptide were mixed at diluted condition (0.01 mM of CaM with 0.03 mM of MB4), and then the sample was gradually concentrated by using ultrafiltration membrane. As a result, I observed the saturation of change in chemical shift of CaM protein at protein: peptide molar ratio of 1:3. From the NMR titration experiment of ^{15}N-labeled CaM with MC5 and MD9 peptide, I also observed the disappearance and emergence of signals indicating the slow exchange timescale of binding of CaM with three peptides. The disappearing and emerging of

cross-peaks were initially observed upon the first point of titration (protein: peptide molar ratio of 1:0.5) and was almost saturated at around a protein: peptide molar ratio of 1:3 (MC5) to 1:4 (MD9).

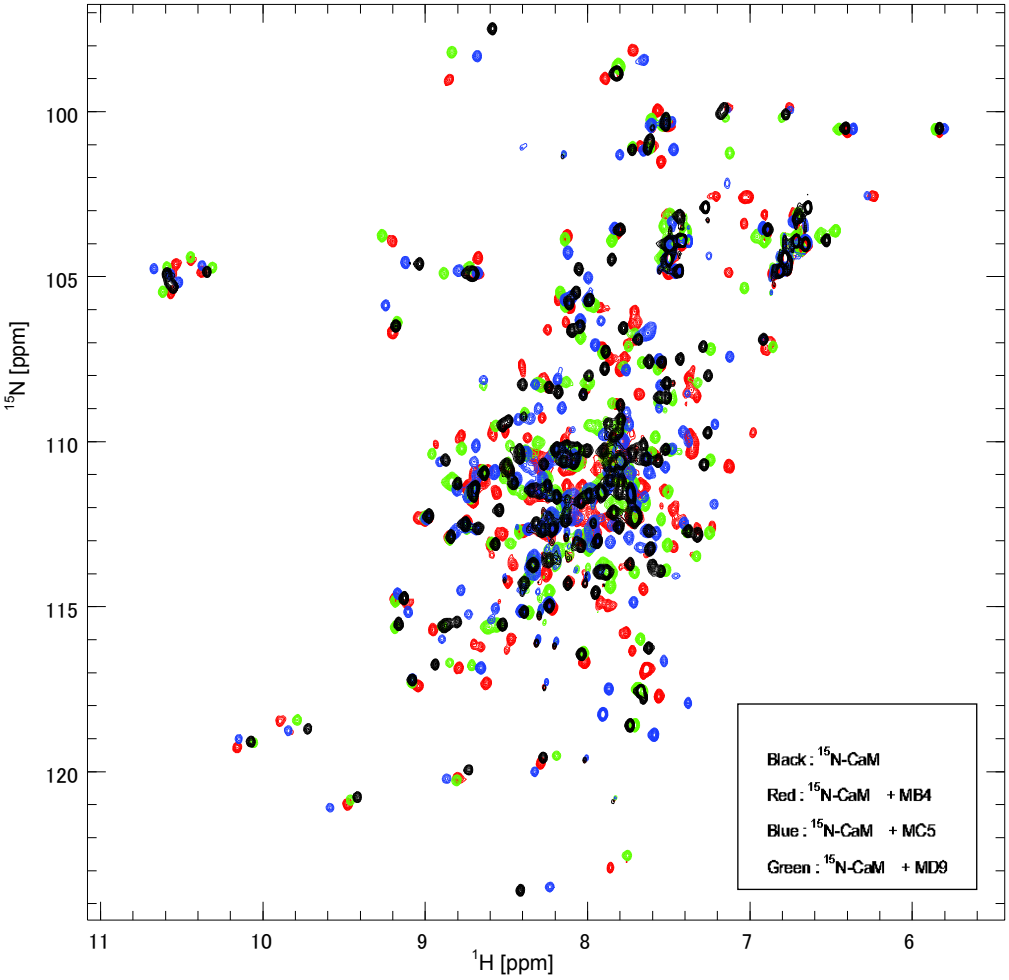

Figure 11: 2D ^{1}H-^{15}N HSQC spectrum

It was found that, large number of CaM resonances were affected by addition of the peptides and the timescale of the binding were slow exchange. It was difficult to follow the tracks of the affected resonances from backbone resonance assignment of free-CaM protein. Therefore, assignment of the backbone ^{1}HN, $^{13}C^{\alpha}$, ^{13}C', ^{15}N and side-chain $^{13}C^{\beta}$ resonances of ^{13}C/^{15}N-uniformly labeled CaM protein in the presence of the peptides were applied. By analyzing the spin-spin connectivity in the 3D

triple-resonance NMR spectra, 67 % of backbone resonances (100 amino acids out of 149 amino acids) were assigned in the presence of MC5 peptide at the protein: peptide molar ratio of 1:3. In the case of MB4 and MD9 peptides, no assignment of the backbone resonance of CaM protein could be done since the quality of 3D NMR spectra were considerably low. This might be due to low solubility of the peptides which caused in the inhomogeneity of the NMR sample and low quality of 3D spectra.

Large chemical shift changes induced by the addition of MC5 peptide (Δ_{ave}> 80 Hz) were found for Ser18, Phe20, Ile28, Val36, Met37, Phe65, from Met73 to Met77, Glu85, Asp94, Lys95, Leu106, Arg107, Met110, Thr111, Lys116, Leu117, Val122, Ileu126, Arg127, Ala129, Asn138, from Glu140 to Met145, which comprise a cluster in a solvent exposed region. The residues affected by addition of MC5 peptide were mapped onto the crystal structure of Rattus rattus CaM[76]. This result indicated that over all region of CaM protein were affected by addition of MC5; however, the changes for Ala129, Asn138 and from Glu140 to Met145 were particularly large and clustered (Figure 12). This result indicated that the cluster of residues including Ala129, Asn138 and from Glu140 to Met145 furnishes the primary binding surface for MC5 peptide (Figure 13). This endows the binding surface for MC5 peptide to be at the C terminal of CaM protein. For the binding surface possibility of MB4 and MD9 peptides, the spectra obtained from 2D NMR were overlaid and was found to resemble the same pattern of chemical shift. Thus, these three peptides have the possibility of binding to the considerably near region of C-terminal domain of CaM protein.

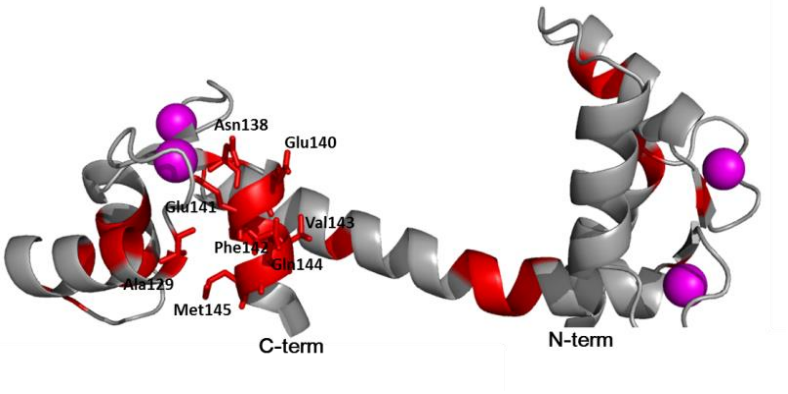

Figure 12: Mapping of the affected residues by addition of MC5 peptide on CaM. Ribbon diagram of CaM showing large chemical shift changes induced by addition of MC5 colored in Red. Ala129, Asn138 and from Glu140 to Met145 represented as stick. Ca^{2+} ions represented as Magenta spheres.

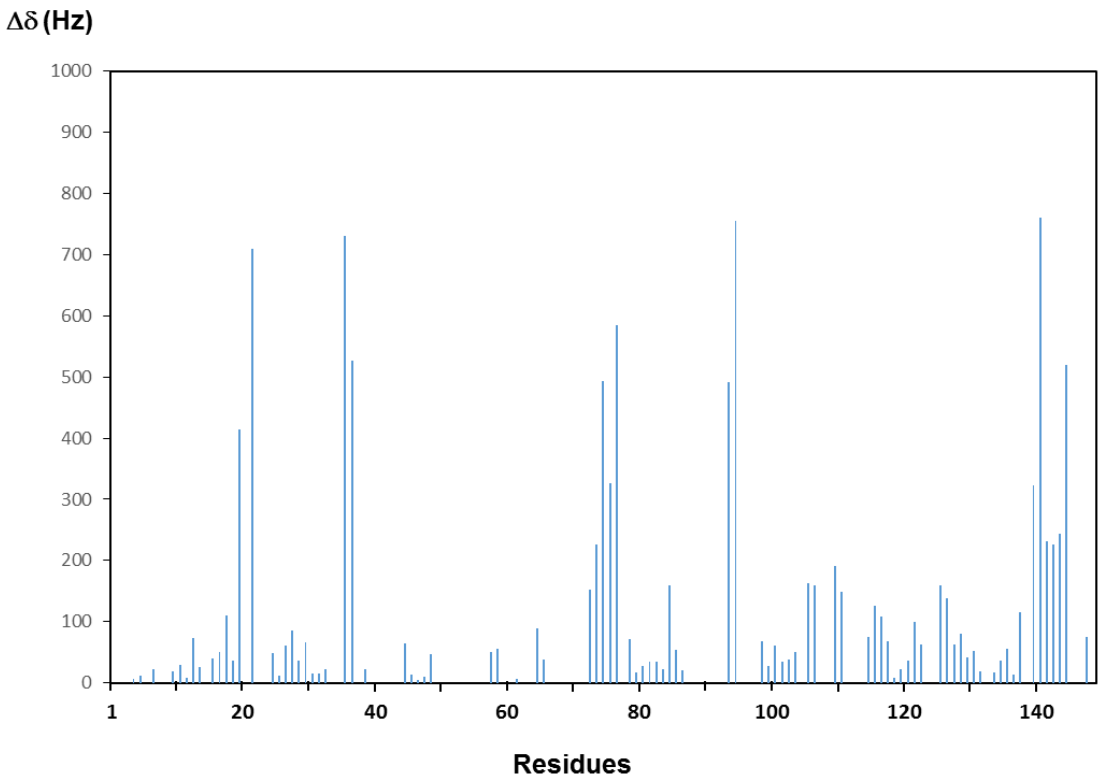

Figure 13: Chemical shift change of CaM by interaction with MC5. The changes in cross-peak were calculated by $[(D^{15}N_{Hz})_2 + (D^{1}H_{Hz})_2]_{1/2}$

3-5 Conclusion

I successfully investigated the detail binding interaction of selected peptides with CaM using fluorescence titration, SPR and NMR measurements. It was found that the addition of five fixed residue on N terminal improve the binding efficiency. The binding affinity from fluorescence titration and SPR was found in nano-molar range. Furthermore, I examine the binding site of the aptamers with 2D NMR and 3D NMR and found that peptide aptamer MC5 has the binding site on C terminal of CaM with high binding affinity.

References

1. Tuerk C and Gold L. Systematic evolution of ligand by exponential enrichment: RNA ligands to bacteriophage T4 DNA polymerase. Science, 249, 1990, pp 505-510.
2. Ellington AD and Szostak JW. *In vitro* selection of RNA molecules that bind specific ligands. *Nature*, 346, 1990, pp 818-822.
3. Smith GP. Filamentous fusion phage: novel expression vectors that display cloned antigens on the virion surface. *Science*, 228, 1985, pp 1315-1317.
4. Hanes J and Pluckthum A. *In vitro* selection and evolution of functional proteins by using ribosome display. *Proc. Natl. Acad. Sci.*, 94, 1997, pp4937-4942.
5. Nemoto N, et al. *In vitro* virus: bonding of mRNA bearing puromycin at the 3'-terminal end to the C-terminal end of its encoded protein on the ribosome *in vitro*. *FEBS Lett.* 414, 1997, pp 405-408.
6. Roberts RW and Szostak JW. RNA-peptide fusions for the *in vitro* selection of peptides and proteins. *Proc. Natl. Acad. Sci.* 94, 1997, pp 12297-12302.
7. Tarasow TM, et al. RNA-catalysed carbon-carbon bond formation. *Nature*, 389, 1997, pp 54-57.
8. Noren CJ, et al. A general method for site-specific incorporation of unnatural amino acids into proteins. *Science*, 244, 1989, pp 182-188.
9. Bain JD, et al. Biosynthetic site specific incorporation of a non-natural amino acid in a polypeptide. *J. Am. Chem. Soc.*, 111, 1989, pp 8013-8014.
10. Uzawa T, et al. "Expansion of aptamer library from “Natural soup” to “Unnatural soup”. *Chem. Commun.*, 49, 2013, pp 1786 – 1795.
11. Liu M, et al. *In vitro* selection of a photo-responsive peptide aptamer by ribosome display. *Chem. Commun.*, 48, 2012, pp 11871-11873.
12. Wang W and et al. A fluorogenic peptide probe developed by *in vitro* selection using tRNA carrying a fluorogenic amino acid. *Chem Commun.*, 50, 2014, pp 2962-2964.

13. Lin YM, et al. Cyclic 3':5'-nucleotide phosphodiesterase -purification, characterization, and active form of protein activator from Bovine brain. *Journal of biological chemistry*. 249, 1974, pp 4943-4954.

14. Crouch TH and Klee CB. Positive Cooperative Binding of Calcium to Bovine Brain Calmodulin. *Biochemistry*, 19, 1980, pp 3692-3698.

15. Sorensen BR and Shea MA. Interactions between domains of apo calmodulin alter calcium binding and stability. *American chemical society*, 37, 1998, pp4244-4253.

16. Osawa M, et al. Solution structure of calmodulin-W-7 complex: the basis of diversity in molecular recognition. *J. Mol. Biol.*, 276, 1998, pp 165-176.

17. Quyang H and Vogel HJ. Metal ion binding to calmodulin: NMR and fluorescence studies. *BioMetals*, 11, 1998, pp 213-222.

18. Liao B, et al. Mechanism of Ca2+-dependent nuclear accumulation of calmodulin. *Proc. Natl. Acad. Sci.*, 96, 1999, pp 6217-6222.

19. Sharma B, et al. Competitive binding assay using fluorescence resonance energy transfer for the identification of calmodulin antagonists. *Bioconjugate Chem.*, 16, 2005, pp 1257-1263.

20. Deswal R and Sopory SK. Glyoxalase from *Brassica juncea* is a calmodulin stimulated protein. *Biochimica et Biophysica Acta*, 1450, 1999, pp 460-467.

21. Luis SM, et al. Natural products with calmodulin inhibitor properties. *Phytochemistry*, 68, 2007, pp 1882-1903.

22. Yao L and Sakaba T. Activity-dependent modulation of endocytosis by calmodulin at a large central synapse. *PNAS*, 109, 2012, pp 291-296.

23. Marietta LB, et al. The early adaptive evolution of calmodulin. *Mol. Biol. Evol.*, 6, 1984, pp 442-455.

24. Thomas JL, et al. Calmodulin binding domains: characterization of a phosphorylation and calmodulin binding site from myosin light chain kinase. *American chemical society*, 25, 1986, pp 1458-1464.

25. Mitsuhiko I, et al. Triple-resonance multidimensional NMR study of calmodulin complexed with the binding domain of skeletal muscle myosin light chain kinase: indication of a conformational change in the central helix. *American chemical society*, 30, 1991, pp 5498-5504.

26. Nevalainen LT, et al. Characterization of novel calmodulin-binding peptides with distinct inhibitory effects on calmodulin-dependent enzymes. *Biochem. J.*, 321, 1997, pp 107-115.

27. Wu X and Reid RE. Structure/ calcium affinity relationships of site III of calmodulin: testing the acid pair hypothesis using calmodulin mutants. *Biochemistry*, 36, 1997, pp 8649-8656.

28. Jhonson JD and Wittenauer LA. A fluorescent calmodulin that reports the binding of hydrophobic inhibitory ligands. *Biochem. J.*, 211, 1983, pp 473-479.

29. Zhou Y, et al. Calcium-dependent association of calmodulin with the Ruvella virus nonstructural protease domain. *The journal of biological chemistry*, 285, 2010, pp 8855-8868.

30. Billingsley LM, et al. A rapid and sensitive method for detection and quantification of calcineurin and calmodulin-binding proteins using biotinylated calmodulin. *Proc. Natl. Acad. Sci.*, 82, 1985, pp 7585-7589.

31. Nichols RA, et al. Calcium/calmodulin-dependent protein kinase II increases glutamate and noradrenaline release from synaptosomes. *Nature*, 343, 1990, pp 647-651.

32. Schulman H and Hanson PI. Multifunctional Ca^{2+}/ calmodulin-dependent protein kinase. *Neurochemical research*, 18, 1993, pp 65-77.

33. Gilchrist JSC, et al. Calcium and calcium-binding proteins in the nucleus. *Molecular and cellular biochemistry*, 135, 1994, pp 79-88.

34. Brown SE, et al. Kinetic control of the dissociation pathway of calmodulin-peptide complexes. *The Journal of Biological Chemistry*, 272, 1997, pp 3389-3397.

35. Rhoads AR and Friedberg F. Sequence motifs for calmodulin recognition. *The FASEB Journal*, 11, 1997, pp331-340.

36. Wang P, et al. Identification of alternative splicing variants of the β subunit of human Ca^{2+}/calmodulin-dependent protein kinase II with different activities. *FEBS Letters*, 475, 2000, pp 107-110.

37. Shahin R and Raha MO. Elaborate ligand-based modeling and subsequent synthetic exploration unveil new nanomolar Ca2+/ calmodulin-dependent protein kinase II inhibitory leads. *Bioorganic and medicinal chemistry*, 20, 2012, pp377-400.

38. Beavo JA, et al. Identification and properties of cyclic nucleotide phosphodiesterases. *Mol Cell Endocrinol*, 28, 1982, pp 387-410.

39. Dedman JR, et al. Physicochemical properties of rat testis Ca^{2+}-dependent regulator protein of cyclic nucleotide phosphodiesterase. Relationship of Ca^{2+}-binding, conformational changes, and phosphodiesterase activity. *J. Biol. Chem.*, 252, 1977, pp 8415-8422.

40. Rossi P, et al. Testis-specific calmodulin-dependent phosphodiesterase. A distinct high affinity cAMP isoenzyme immunologically related to brain calmodulin-dependent cGMP phosphodiesterase. *J. BIol. Chem.*, 263, 1988, pp 15521-15527.

41. Goraya TA and Cooper DMF. Ca^{2+}-calmodulin-dependent phosphodiesterase (RDE1): current perspectives. *Cellular signaling*, 17, 2005, pp 789-797.

42. Jones HP, et al. Calmodulin-dependent stimulation of the NADPH oxidase of human neutrophils. *Biochim Biophys Acta*, 714, 1982, pp 152-156.

43. Watterson DM, et al. Structural similarities between the Ca^{2+}-dependent regulatory proteins of 3':5'-cyclic nucleotide phosphodiesterase and actomyosin ATPase. *J Biol Chem*, 251, 1976, pp 4501-4513.

44. Blum JJ, et al. Calmodulin confers calcium sensitivity on ciliary dynein ATPase. *J Cell Biol*, 87, 1980, pp 386- 397.

45. Wolff DJ, et al. Calcium-dependent cyclic nucleotide phosphodiesterase from brain identification of phospholipids as calcium-independent activators. *Arch. Biochem. Biophys.*, 173, 1976, pp 720-731.

46. Pierce HH, et al. Identification of cyclized calmodulin antagonists from a phage display random peptide library. *Molecular diversity*, 1, 1995, pp259-265.

47. Vetter SW and Leclerc E. Novel aspects of calmodulin target recognition and activation. *Eur. J. Biochem.*, 270, 2003, pp 404-141.

48. Wu X and Bers DM. Free and bound intracellular calmodulin measurements in cardiac myocytes. *Cell Calcium*, 41, 2007, pp 353-364.

49. Hayashi N, et al. Myristoylation-regulated direct interaction between calcium-bound calmodulin and N-terminal region of pp60. *J.Mol.Biol.*, 338, 2004, pp 169-180.

50. Adey NB and Kay BK. Identification of calmodulin-binding peptide consensus sequences from a phage-displayed random peptide library. *Gene*, 169, 1996, pp 133-134.

51. Dedman JR, et al. Selection of target biological modifiers from a bacteriophage library of random peptides: The identification of novel calmodulin regulatory peptides. *J. Biol. Chem.*, 268, pp 23025-23030.

52. Shen X, et al. Scanning the human proteome for calmodulin-binding proteins. *PNAS*, 102, 2005, pp 5969-5974.

53. Kajihara D, et al. Synthesis and sequence optimization of GFP mutants containing aromatic non-natural amino acids at the Try66 position. *Protein Eng Des* Sel. 18, 2005, pp 273-277.

54. Iijima I and Hohsaka T. Position-specific incorporation of fluorescent non-natural amino acids into maltose-binding protein for detection of ligand binding by FRET and fluorescence quenching. *Chembiochem*, 10, 2009, 999-100

55. Taira H, et al. Comprehensive screening of amber suppressor tRNAs suitable for incorporation of non-natural amino acids in a cell-free translation system. *Biochem Biophys Res Commun*, 374, 2008, 304-308.

56. Wada A, et al. Ribosome display selection of a metal-binding motif from an artificial peptide library. *Biotechnol Bioeng*, 101, 2008, pp 1102-1107.

57. Wang W, et al. Polypeptide aptamer selection using a stabilized ribosome display. *J Biosci Bioeng*., 112, 2011, pp 515-517.

58. Novotny J. Synthesis of fluorescence C(24)-ceramide: Evidence for acyl chan length dependent differences in penetration of exogenous NBD-ceramides into human skin. *Bioorg Med Chem Lett*, 19, 2009, pp 6975-6977.

59. Lin YM, et al. Cyclic 3'-5'-Nucleotide phosphodiesterase- purification, characterization and active form of protein activator from Bovine brain. *Journal of biological chemistry*, 249, 1974, pp 4943-4954.

60. Crouch TH and Klee CB. Positive cooperative binding of calcium to Bovine brain Calmodulin. *Biochemistry*, 19, 1980, 3692-3698.

61. NMR ref http://www.bio.cam.ac.uk/azara/

62. Vranken WF, et al. The CCPN data model for NMR spectroscopy: development of a software pipeline. *Proteins*, 59, 2005, pp 687-696.

63. Hayashi N, et al. An expression system of rat calmodulin using T7 phage promoter in Escherichia coli. *Protein Expr Purif*, 12, 1998, pp 25-28.

64. Schanda P and Brutscher B. Very fast two-dimensional NMR spectroscopy for real-time investigation of dynamic events in proteins on the time scale of seconds. *J Am Chem Soc*, 127, 2005, pp 8014-8015.

65. Barna JCJ, et al. Exponential Sampling, an Alternative Method for Sampling in Two-Dimensional NMR Experiments. *Journal of Magnetic Resonance*, 73, 1987, pp 69-77.

66. Schmeider P, et al. Improved Resolution in Triple-Resonance Spectra by Nonlinear Sampling in the Constant-Time Domain. *Journal of Biomolecular NMR*, 4, 1994, pp 483-490.

67. Rovnyak D, et al. Accelerated acquisition of high resolution triple-resonance spectra using non-uniform sampling and maximum entropy reconstruction. *Journal of Magnetic Resonance*, 170, 2004, pp 15-21.

68. Ikeya T, et al. NMR protein structure determination in living E. coli cells using nonlinear sampling. *Nature Protocols*, 5, 2010, pp 1051-1060.

69. Laue ED, et al. Reconstruction of phase-sensitive two-dimensional NMR-spectra by maximum-entropy. *Journal of magnetic resonance*, 14, 1986, pp 1262-1263.

70. Zielinski RE. Calmodulin and calmodulin-binding proteins in plants. *Annu. Rev. Plant Physiol. Plant Mol. Biol.*, 49, 1998, pp 697-725.

71. http://www.uniprot.org/uniprot/P17677#section_seq

72. http://www.uniprot.org/uniprot/Q92686#section_seq

73. http://www.uniprot.org/uniprot/Q05682

74. Rhoads AR and Friedberg F. Sequence motifs for calmodulin recognition. *The FASEB Journal*, 11, 1997, pp 331-340.

75. http://www.proteinstructures.com/Structure/Structure/amino-acids.html

76. 10.2210/pdb3cln/pdb

CHAPTER 4

CONCLUSIONS

This thesis illustrate the design, development and study of fluorescent signaling peptide aptamers using ribosome display *in vitro* selection technique. *In vitro* selection and interaction of verotoxin binding peptide aptamers and binding interactions of CaM selected peptide aptamers are conferred in detail.

In chapter 1, the general introduction is given related to the research work carried out including the background information, techniques used for the study, and its application.

In chapter 2, the selection of signaling peptide aptamer by molecular evolutionary engineering technique was successfully conducted. The selected peptide aptamer against verotoxin showed the decrease in fluorescence intensity by 78% on interaction with protein at saturated level. The interaction found was highly specific with the binding affinity 3.9 μM. Thus the developed peptide aptamer can be used for the detection of verotoxin.

In chapter 3, the detail binding interaction was carried out for the CaM selected peptide aptamer by adding five fixed residue on N terminal. The result obtained from the fluorescence titration, SPR and NMR measurements showed that addition of five fixed residue on N terminal improve binding affinity. The binding affinity from fluorescence titration and SPR was found in nano-molar range. As well binding site was found on C terminal of CaM from the 2D NMR and 3D NMR investigation.

The studies carried out in this thesis disclose that ribosome display is a prevailing technique in developing fluorescent signaling peptide aptamers. The selected aptamers have potential to develop a diagnosis tool for verotoxin detection and biosensor to understand about the Ca^{2+} modulated signaling protein CaM.

Acknowledgements

This doctoral dissertation is a compilation of work carried out at Nano Medical Engineering Laboratory, RIKEN, during 2012-2015.

Foremost, I would like to express my sincere thanks and gratitude to Professor Yoshihiro Ito for giving me the opportunity of pursuing PhD at Tokyo Metropolitan University. I am extremely grateful for his professional guidance, intellect input, time, encouragement, scientific support and constructive criticism during the research. I am fortunate to have been able to work in his laboratory at RIKEN.

I express my heartful gratitude to Professor Toshiro Aigaki, an optimistic and friendly supervisor who supported and trusted on my research.

I thank Dr. Takanori Uzawa, my mentor in the lab. His advice was immensely useful. His willingness to teach me techniques outside my discipline was invaluable, and helped take this research to a level that may not have otherwise been possible. I would also like to express my sincere gratitude to Professor Yutaka Ito, Professor Nobuhiro Hayashi and Dr. Jin Inoue who helped to create a productive result in the NMR assignments.

Thanks to my senior Dr. Wei Wang for being extremely generous and supporting me with best guidelines in the research. Many thanks to my dear friend and co graduate student Quan Xiuming, who made my life in the university easy and enjoyable.

I appreciate the financial support by Junior Research Associate (JRA) program for graduate students from the research personnel support section, Global Relation Office, RIKEN.

I am extremely thankful for the patience, support and understanding of my

loving husband, Tara Bahadur KC who kept me sane even in the time of happiness or stress in research. Special gratitude to Mr. Om Krishna Manandhar and Ms. Gauri Manandhar (my parents), who always nurtured and supported education financially and morally. I owe my deepest respect to my brother Mr. Sanjay Manandhar and my sister in law Ms. Sudarshana Manandhar for their enmorous love, encouragement and assistance. Last but not the least, I am thankful to everyone with whom I worked for your unconditionally love which makes me proud of myself no matter what I accomplished.

Appendix

NMR spectrum of NBDaa

Appendix 1: ^{1}H-NMR spectrum of NBDaa

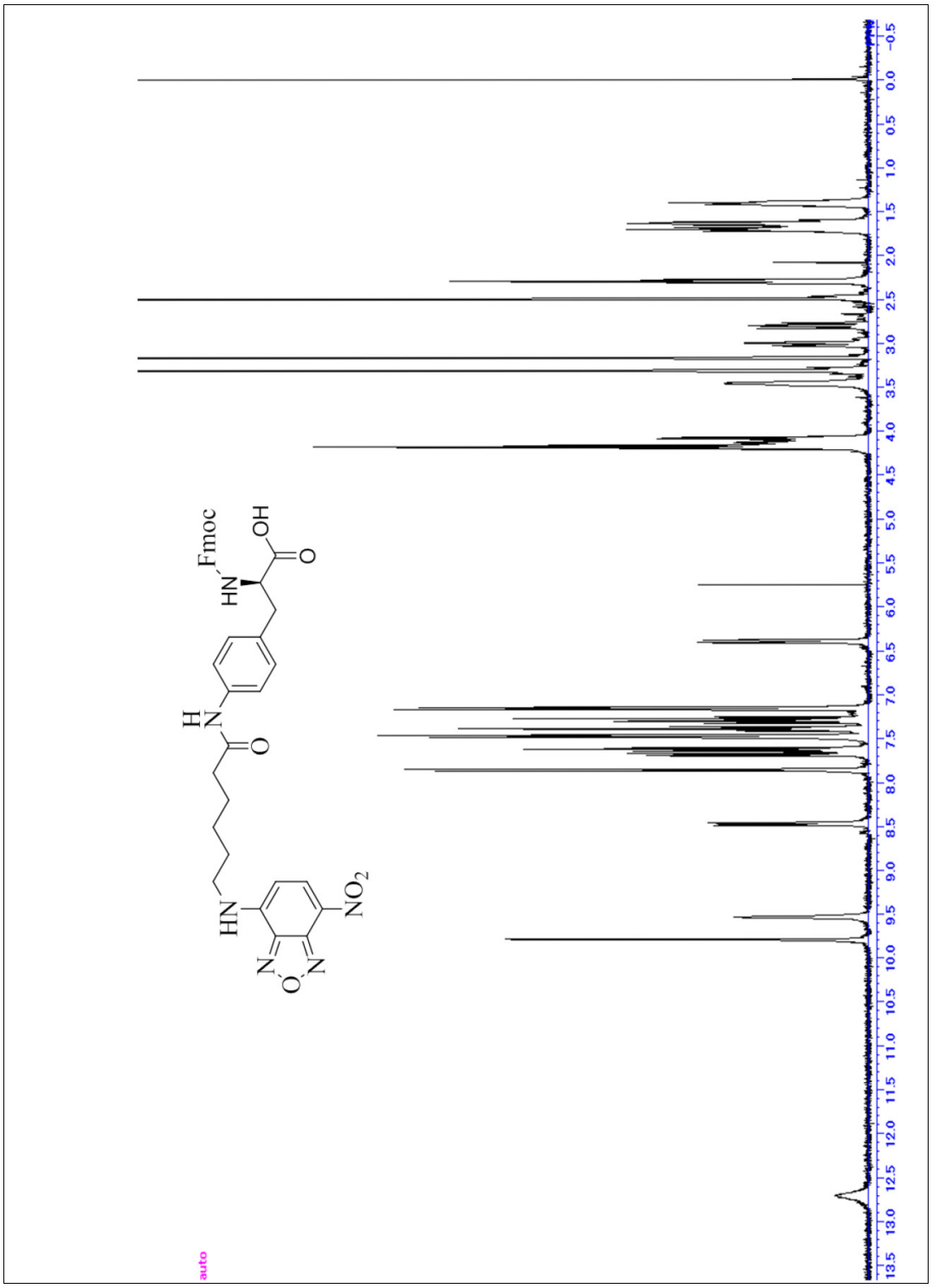

Appendix 2: Aromatic protons of NBDaa

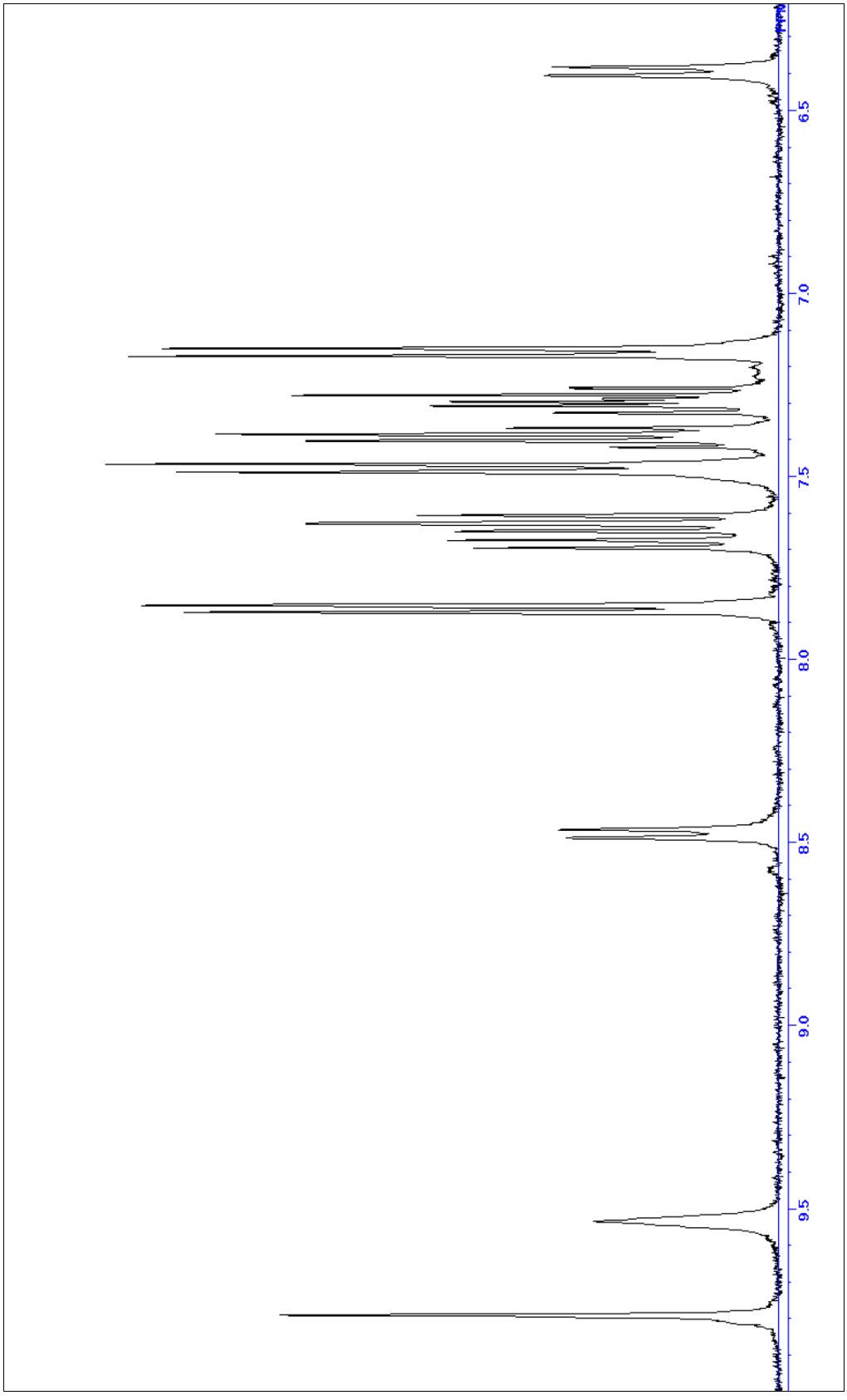

Appendix 3: ^{13}C-NMR of NBDaa

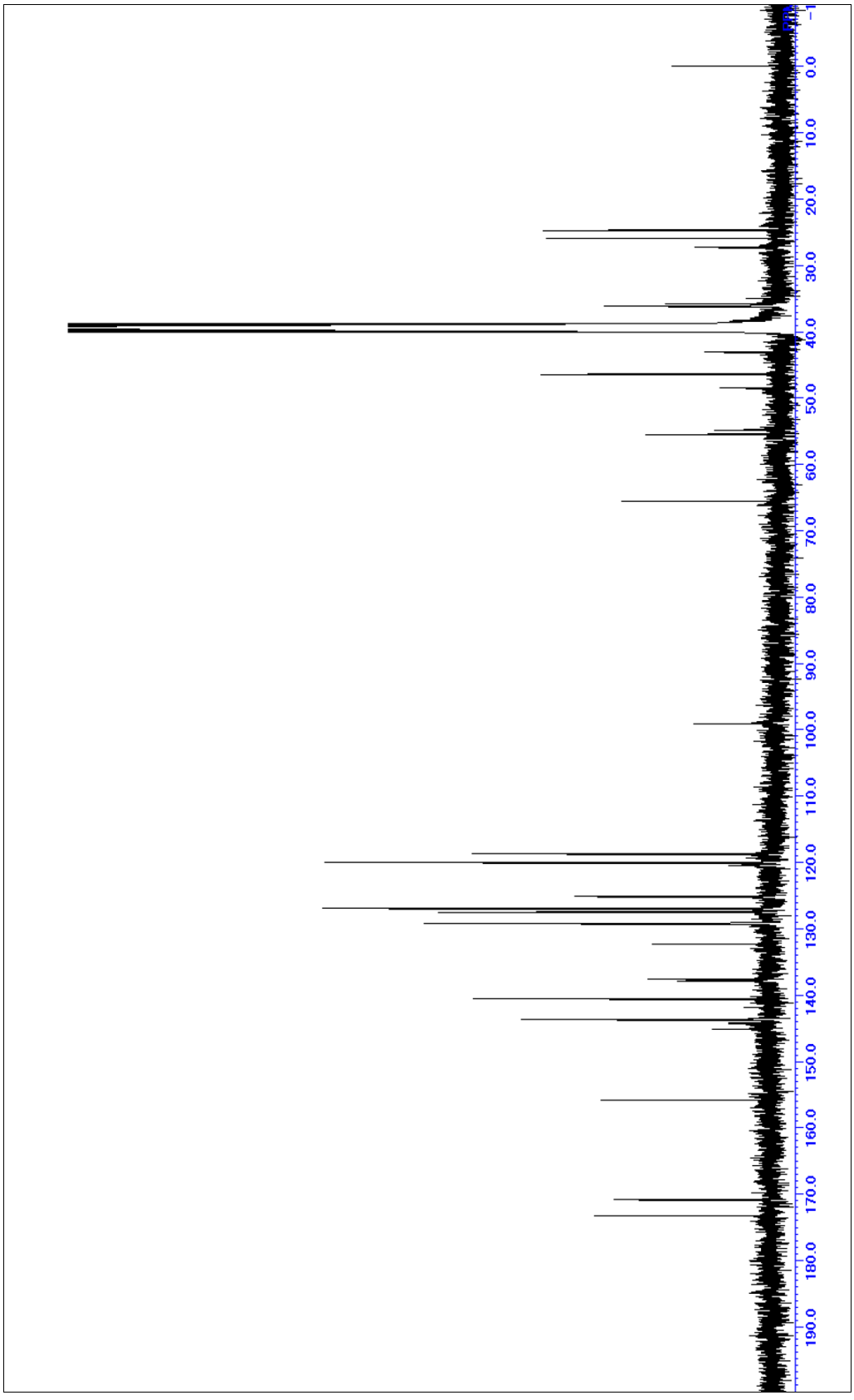

MALDI-TOF-MS spectrum of NBDaa

Appendix 4: MS spectrum of NBDaa (Calculated M+Na: 701.24)

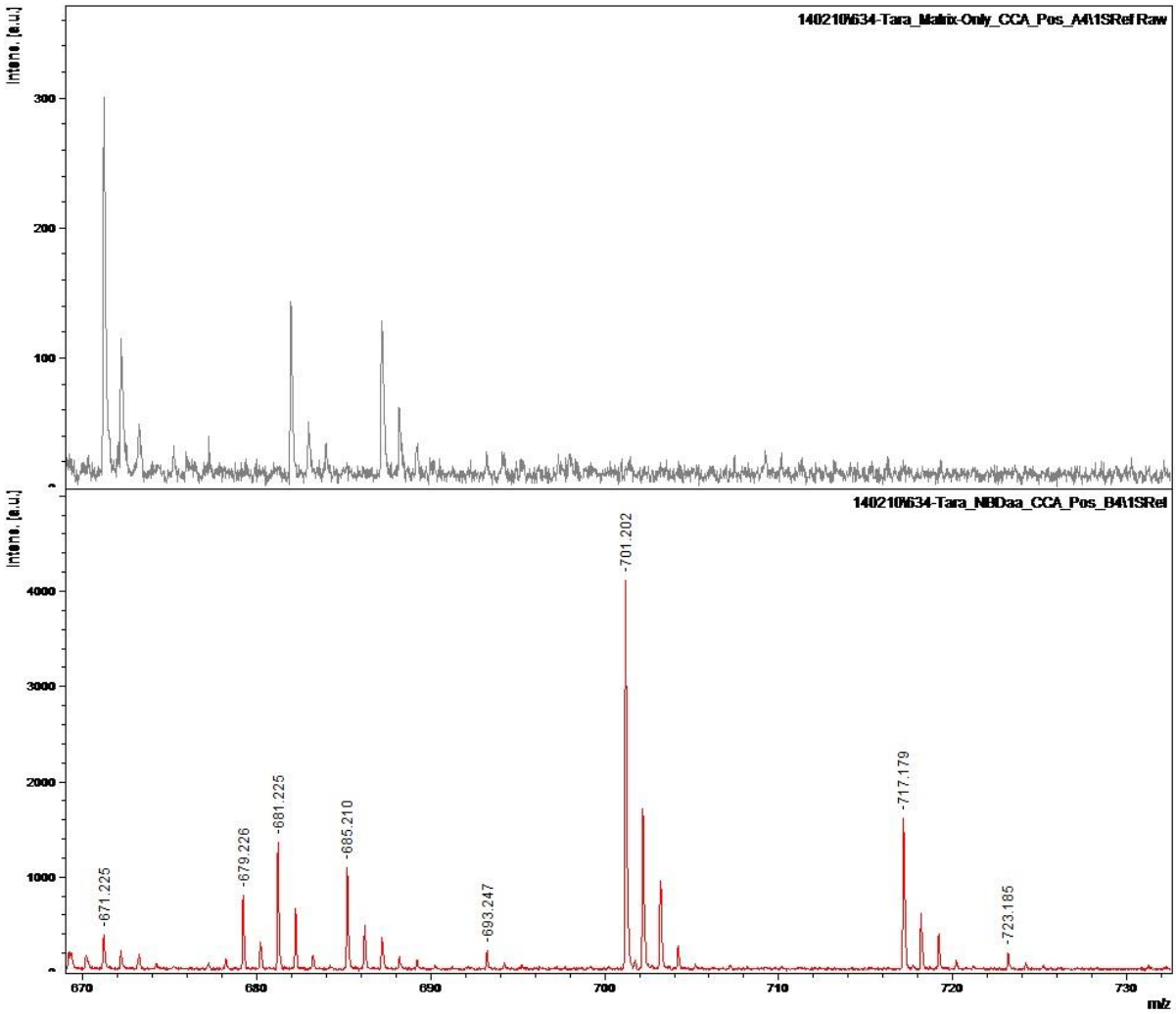

HPLC analysis spectrum of peptides selected against verotoxin.

Appendix 5: HPLC analysis of peptide VT4

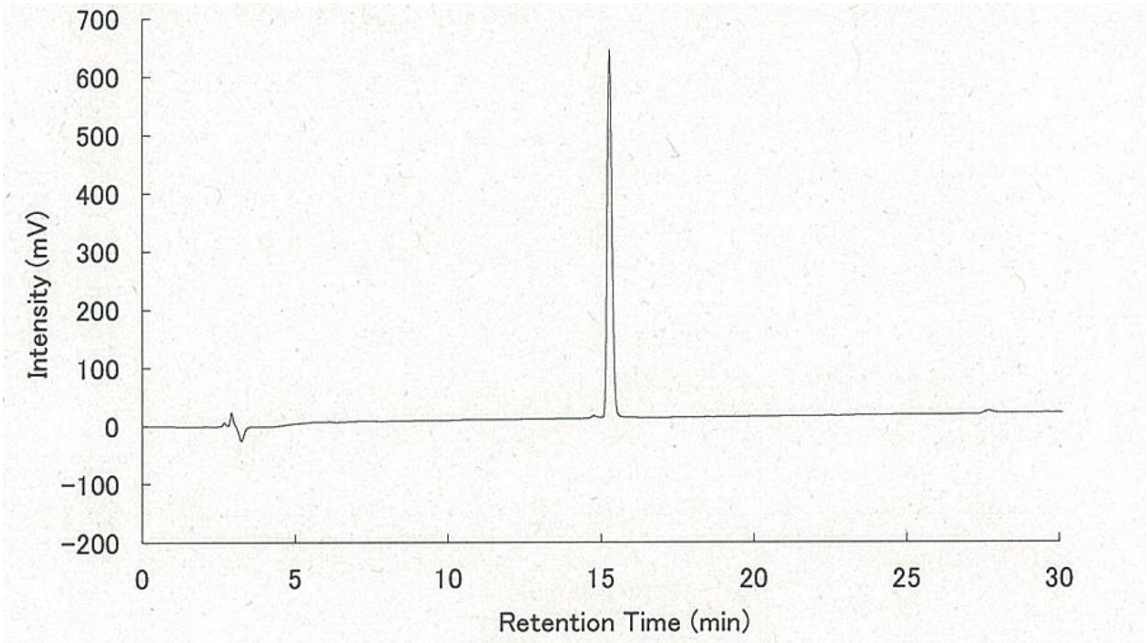

HPLC conditions :

Column,	Inertsil ODS-3 (250 x 4.6 mm I.D.)	Column temp.,	25 ℃
Mobile phase,	30-60% CH_3CN (contg. 0.1% TFA) (30 min)		
Flow rate,	1.0 mL/min	Detection,	UV at 215 nm
		Purity :	97.6%

MALDI-TOF-MS spectrum of peptides selected against verotoxin.

Appendix 6: MS spectrum of peptide VT4 (Calculated M+H: 1733)

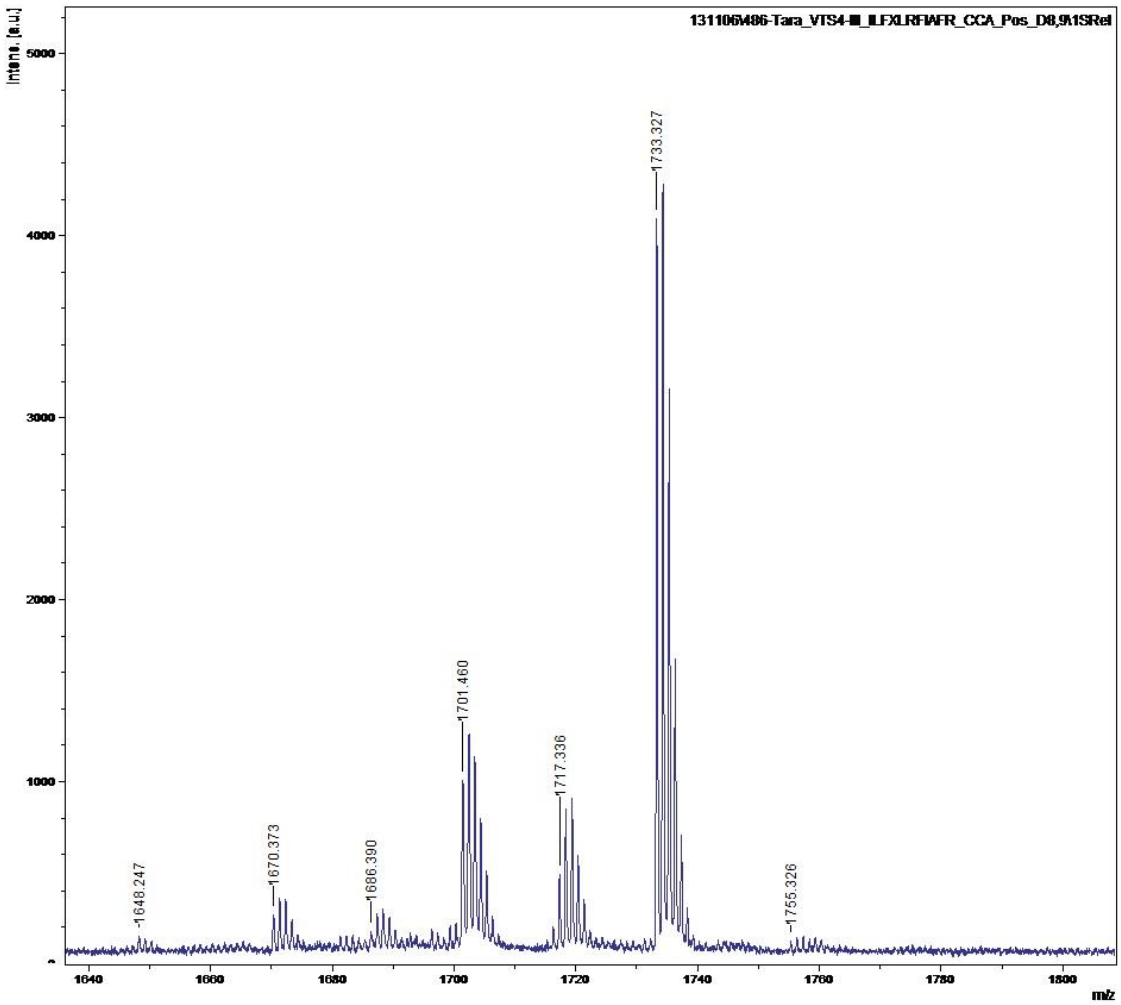

HPLC analysis spectrum of peptides selected against CaM.

Appendix 7: HPLC analysis of peptide MA4

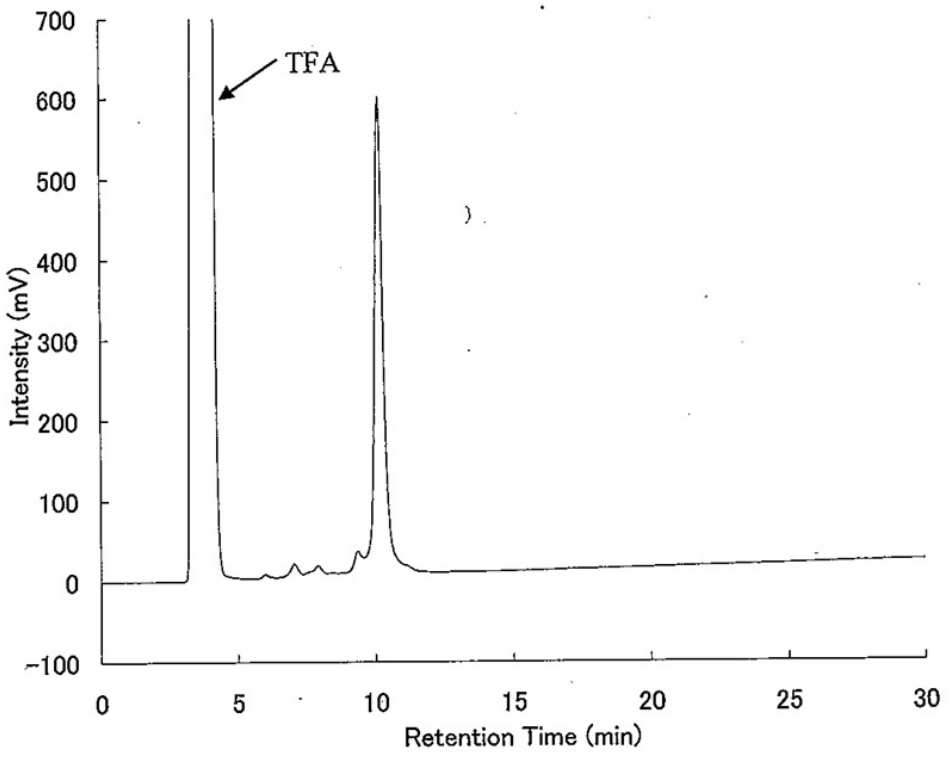

Purity : 89.5%

HPLC conditions :

Column,	YMC-Pack PROTEIN-RP (250 x 4.6 mm I.D.)
Column temp.,	25 ℃
Mobile phase,	30-60% CH_3CN (contg. 0.1% TFA) (30 min)
Flow rate,	1.0 mL/min
Detection,	UV at 215 nm

Appendix 8: HPLC analysis of peptide MB4

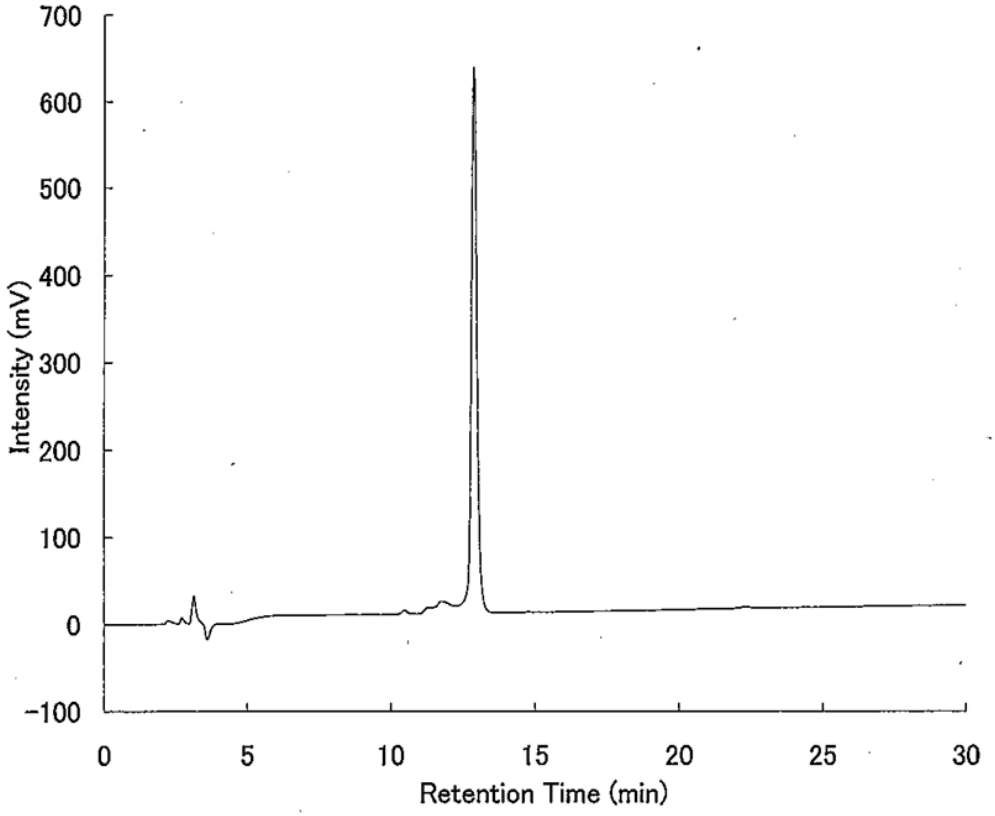

Purity : 91.4%

HPLC conditions :

Column,	Inertsil ODS-3 (250 x 4.6 mm I.D.)
Column temp.,	25 ℃
Mobile phase,	20-50% CH_3CN (contg. 0.1% TFA) (30 min)
Flow rate,	1.0 mL/min
Detection,	UV at 215 nm

Appendix 9: HPLC analysis of peptide MC5

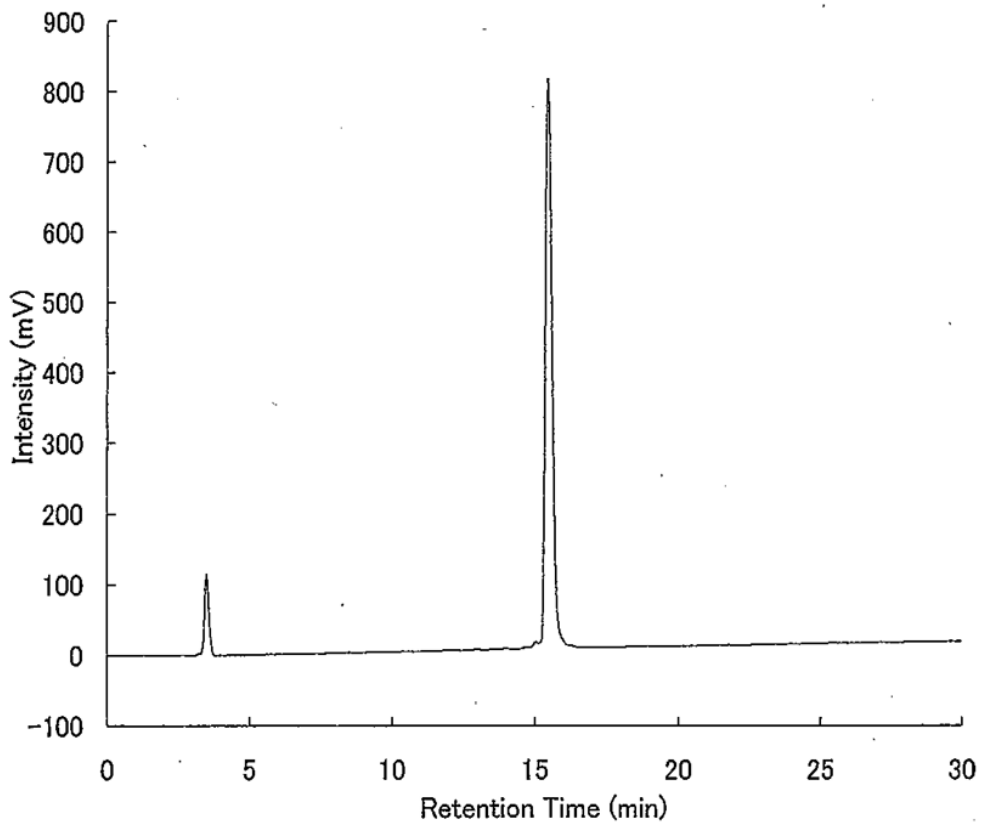

Purity : 97.2%

HPLC conditions :

Column,	YMC-Pack PROTEIN-RP (250 x 4.6 mm I.D.)
Column temp.,	25 ℃
Mobile phase,	25-55% CH_3CN (contg. 0.1% TFA) (30 min)
Flow rate,	1.0 mL/min
Detection,	UV at 215 nm

Appendix 10: HPLC analysis of peptide MD9

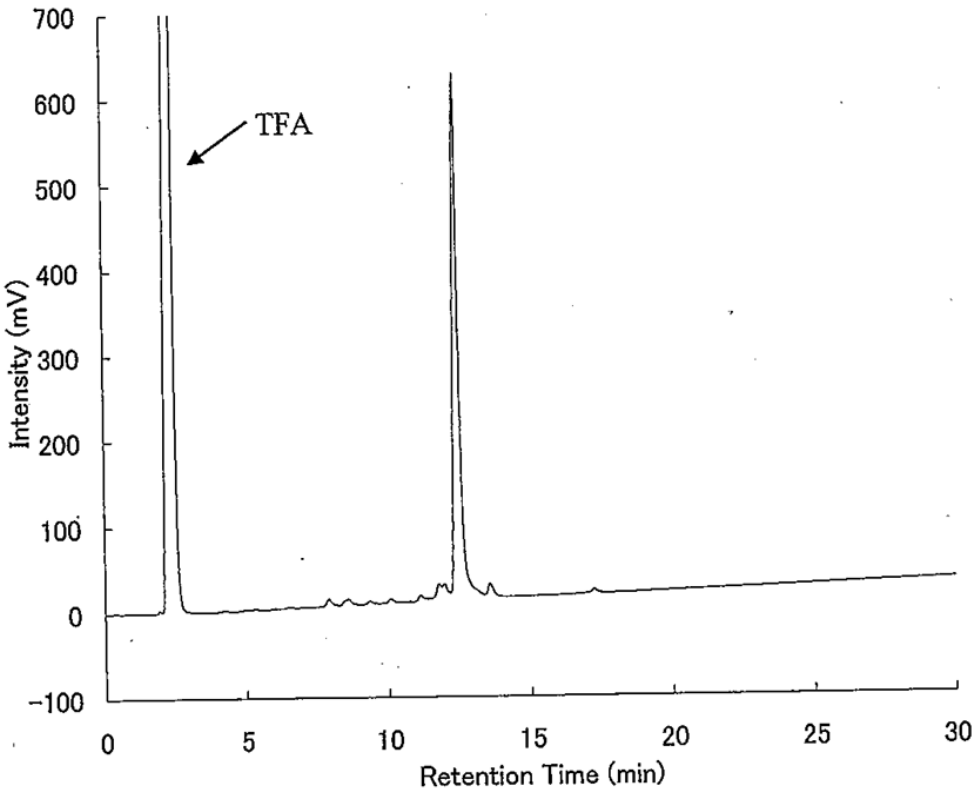

Purity : 85.0%

HPLC conditions :

Column,	Hipep-Intrada RP (150 x 4.6 mm I.D.)
Column temp.,	25 ℃
Mobile phase,	25-55% CH_3CN (contg. 0.1% TFA) (30 min)
Flow rate,	1.0 mL/min
Detection,	UV at 215 nm

List of Publications

Original papers

1. **Yasodha Manandhar**, Tara Bahadur K.C., Wei Wang, Takanori Uzawa, Toshiro Aigaki and Yoshihiro Ito. "*In vitro* selection of a peptide aptamer that changes fluorescence in response to verotoxin", ***Biotechnol Lett***, 2014, DOI: 10.1007/s10529-014-1719-7, pp 1-7.
2. **Yasodha Manandhar**, Wei Wang, Jin Inoue, Takanori Uzawa, Nobuhiro Hayashi, Yutaka Ito, Toshiro Aigaki and Yoshihiro Ito. "Interactions of *in vitro* selected fluorogenic peptide aptamers with calmodulin". (Under preparation)

Poster presentation

1. **Yasodha Manandhar**, Tara Bahadur K.C., Wei Wang, Takanori Uzawa, Toshiro Aigaki and Yoshihiro Ito. "*In vitro* selection of a peptide aptamer that changes fluorescence in response to verotoxin". University of Seoul, February, Seoul, South Korea.
2. **Yasodha Manandhar**, Tara Bahadur K.C., Wei Wang, Takanori Uzawa, Toshiro Aigaki and Yoshihiro Ito. "*In vitro* selection of a peptide aptamer that changes fluorescence in response to verotoxin". Noyori School 2014, December, Hyama, Japan.
3. **Yasodha Manandhar**, Takanori Uzawa, Toshiro Aigaki and Yoshihiro Ito. "*In vitro* selection of peptide aptamer binding to reduced ferredoxin". The 51st Annual Meeting Biophysical Society of Japan, Kyoto, Japan (2013).
4. **Yasodha Manandhar**, Takanori Uzawa, Toshiro Aigaki and Yoshihiro Ito. "*In vitro* selection of peptide aptamer binding to reduced ferredoxin". Noyori Summer School 2013, September, Kobe, Japan.

5. **Yasodha Manandhar**, Wei Wang, Takanori Uzawa, Toshiro Aigaki and Yoshihiro Ito. "Fluorescence Titration for finding the binding sites of Peptide Aptamers on Calmodulin". The 50th Annual Meeting Biophysical Society of Japan, Nagoya, Japan (2012).
6. **Yasodha Manandhar**, Wei Wang, Takanori Uzawa, Toshiro Aigaki and Yoshihiro Ito. "Fluorescence Titration for finding the binding sites of Peptide Aptamers on Calmodulin". Noyori Summer School 2012, October, Shimane, Japan.